Earth And Planetary Science Letters
December 2019, Volume 528 Pages 115851 (14p.)
https://doi.org/10.1016/j.epsl.2019.115851
https://archimer.ifremer.fr/doc/00586/69822/

Triple oxygen isotope investigation of fine-grained sediments from major world's rivers: Insights into weathering processes and global fluxes into the hydrosphere

Bindeman Ilya N. [1, 2, *] , Bayon Germain [3], Palandri James [1]

[1] Department of Earth Sciences, University of Oregon, Eugene, OR 97403-1272, USA
[2] Sciences de la Terre et de l'Environnement, Université de Genève, rue des Maraîchers 13, CH-1205 Genève, Switzerland
[3] IFREMER, Marine Geosciences Unit, F-29280 Plouzané, France

* Corresponding author : Ilya N. Bindeman, email address : bindeman@uoregon.edu

Abstract :

Continental weathering is accompanied by formation of clays and other secondary minerals and their δ18O and D17O values should hence reflect to some extent signatures of meteoric water (δ18OMW) and mean annual temperatures (MAT). Our ability to extract climate information from weathered products across the geologic history relies on analytical methods tested and calibratedagainst modern climate conditions. We here present triple-oxygen isotope analyses of clay-size sediments from 45 rivers worldwide, as well as δ18O analyses of corresponding silt- and sand rich detrital fractions, which altogether cover about 25% of the continental area that drained into the oceans, extending from the tropics to polar regions. The majority of studied clays closely approximate weathering products, always having high-δ18O signatures regardless of the bedrock type, and in equilibrium with local meteoric waters. Silts are only ~1.9‰ lighter on average due to greater detrital dilution. Overall, bulk clays from across different climatic regions do no vary much isotopically; an observation which we attribute to opposing effects of temperature on clay water fractionation and hydrologic relationship between temperature and δ18OMW. Mathematical inversion of measured clay δ18O and D17O values (corrected for detrital contribution) into MAT and δ18OMW, compiled for each studied watershed, returns satisfactory estimates. Globally, triple O isotopes in clays appear to be water-dominated, being controlled almost exclusively by δ18OMW at respective temperature of weathering, with minor effects related to evaporation. Using sand from rivers, correlation of δ18O silts with detrital proportions, and estimated surface outcrop of different rock types, we additionally arrive at a +11.5‰ estimate for the exposed silicate crust undergoing weathering.

Globally-averaged, sediment-flux weighted clay δ18O and D17O values are +14.80‰ and - 0.164‰, respectively. These values are significantly skewed toward O isotope signatures for the southeast Asia and western Pacific regions, characterized by very high sediment fluxes to the ocean. Using both clay- and silt-size fractions, the total weighted silicate weathering δ18O signature exported to the world's ocean

is -2.59‰, almost 50% higher the previous estimate, yielding an ice-free world hydrosphere estimate of -0.78‰.

Overall, the modern river clays represent a snapshot of modern weathering conditions on continents, and associated first-order climatic signatures related to MAT and δ18O of the hydrosphere. This implies that measured increase in δ18O and stepwise decrease in D17O in shales in the geologic record capture: evolving global hydrologic cycle upon continental emergence, decrease in global MAT or diagenetic conditions, and decreasing ocean mass via rehydrating of the mantle by subduction of hydrated low-δ18O, high-D17O slabs.

Highlights

► Little global variation of δ18O and D17O in bulk clays and silts from 45 world rivers. ►They individually record the isotopic composition of regional precipitation and *T*. ► Total weathering flux to hydrosphere is 50% higher than previous estimate. ► Global silicate surface is +11.5‰ but bedrock influence on δ18O in clays is minimal. ► Ice-free ocean is estimated $\delta^{18}O = -0.78$ ‰ and $D'^{17}O = -0.0168$ ‰.

Keywords : triple oxygen isotopes, weathering, hydrosphere evolution, clay minerals

1. Introduction

1.1. Importance of clays for paleoclimate research

Geochemical investigations of modern or ancient Earth surface materials, such as mudrocks or shales, provide valuable information about the composition of the paleo-atmosphere and hydrosphere, continental weathering processes (Holland, 1984; Retallack, 2006; Farquhar and Wing, 2005; Lyons et al., 2014), and the evolution of the the average composition of the continental crust through time (Goldschmidt, 1933; Wedepohl, 1995; Rudnick and Gao, 2003;

57 Greber et al., 2017). On a global scale, clays and other weathering products account for about
58 two-thirds of the volume of the mudrocks and shales (Shaw and Weather, 1965; Pettijohn, 1957;
59 Ronov and Yaroshevsky, 1969) derived from the eroding continents. In this study, we apply
60 newly-developed triple-oxygen isotopic methods and report data for modern clay-size detrital
61 minerals transported by rivers. As weathering proceeds with a great excess of water, oxygen and
62 hydrogen isotopic compositions of newly formed clays on continents could record corresponding
63 meteoric water signatures and the temperature of interaction during weathering (Holland, 1984;
64 Bindeman et al., 2016; 2018). Likewise, unaltered mudrocks and shales in the geologic record
65 retain similar information with some complications. The diagenetic transformation of mudrocks
66 into shales involves water expulsion during the smectite/illite transition, leading to minor shifts
67 in $\delta^{18}O$ and more significant shifts in δD (Yeah and Savin, 1976,1977; Land and Lynch, 1997)
68 that likely affect temperature estimates. Yeh and Savin (1976) demonstrated with marine
69 sediments that clay residence times of up to 10^6-10^7 yr in cold ~0‰ seawater does not affect
70 their O and H isotopic values acquired during weathering.
71 Studies of "conventional" O and H stable isotopic variations in clays, sediments, and
72 mudrocks span the last 70 years or so (Silverman, 1951; Savin and Epstein, 1970a,b; Lawrence
73 and Taylor, 1971). Savin and Lee (1988), and Sheppard and Gilg (1996) experimentally and
74 empirically constrained clay-water fractionation factors for individual clay minerals. Using these,
75 recent investigations of O and H stable isotopic variations in pristine monomineralic clays have
76 aimed at providing constraints on paleoaltimetry, isotopic rain shadows, continental drift, and
77 transition from wet to arid climates (Savin and Hsieh, 1998; Mulch et al., 2008; Mix and
78 Chamberlain, 2014).
79 Traveling deeper into the geologic time, a key unresolved question concerns the
80 evolution of the global $\delta^{18}O$ seawater in the past. On 10^7 yr timescales, it is thought to be mainly
81 controlled by continental weathering inputs, related to global climate conditions; and the
82 intensity of low- and high-T water-rock interactions at mid-ocean ridges, which relate to global
83 spreading rates (Holland, 1984; Muehlenbachs, 1998; Kasting et al., 2006; Sengupta and Pack,

2018; Zakharov and Bindeman, 2019). Recently, we applied the new $\Delta^{17}O$ proxy to shales and weathering products, to better constrain weathering and associated hydrosphere conditions in the geologic past (Bindeman et al., 2016; 2018). In particular, we observed a first order trend of $\delta^{18}O$ increasing towards most recent times, punctuated by 2^{nd}- order variations over a 0.5-1 Ga timescales, that we explained by both supercontinent cycles and global perturbations such as Snowball Earth climate episodes. Furthermore, a step-wise change in $\Delta^{17}O$ at 2.4Ga was identified, interpreted as evidence of the diversification of the meteoric water cycle due to the rapid appearance of wide continental areas above sea level (Bindeman et al., 2018), leading to weathering conditions comparable to modern. Here, our main aim was to calibrate these new proxies against modern climatic conditions, using recent sediment samples with known T and isotopic values of formation waters.

1.2 Weathering reactions and clay production

Fine-grained weathering products such as clays are transported by rivers from soils to depositional environments, providing averaged geochemical compositions of corresponding watersheds and drainage basins. We analyzed a series of clay-size and silt-size sediments, derived from 45 river basins around the world (**Fig. 1**). The same series of samples has been previously characterized for XRD mineralogy, major and trace element compositions, and neodymium, hafnium, and silicon isotopes (Bayon et al., 2015;2016;2018). The studied samples correspond to modern river bank sediments or recent (core-top) sediment samples recovered at continental margins near the mouths of rivers, deltas, estuaries, or upstream river waters.

On continents, weathering of silicate rocks proceeds with depletion of alkaline elements and calcium, followed by silica removal, leading to overall enrichment in Al in secondary neo-formed clays (Retallack, 2001). As a consequence, Al-based indices of alteration, such as the Chemical Index of Alteration (CIA; Nesbitt and Young, 1982), or Al/Si ratios typically serve as a measure of weathering intensity. Weathering reactions such as feldspar breakdown proceed as follow:

111

$$CaAl_2Si_2O_8 + H_2O + 2H^+ + CO_3^{2-} = Al_2Si_2O_5(OH)_4 + CaCO_3 \quad [1]$$

Feldspar *Kaolinite* *Calcite*

CIA=50 CIA=100

115

116 As oxygen is exchanged in these reactions, the products carry an isotopic record of time-
117 integrated weathering waters $\delta^{18,17}O_{WW}$ and temperatures:

$$\delta^{18,17}O_{\text{weathering product}} = \delta^{18,17}O_{MW}{}^{f(T)} + \Delta_{MW\text{-}WW} + \Sigma_{i..j} (\Delta_{\text{mineral-MW}})^{f(T)} \cdot W_{i..j} \quad [2]$$

118

119 where $W_{i..j}$ are weighting factors of individual mineral proportions, and $\Delta_{\text{mineral-MW}}$ are
120 fractionation factors ($\delta^{18,17}O_{min} - \delta^{18,17}O_{water} = \Delta_{\text{mineral-MW}} \approx 1000 \ln\alpha_{\text{mineral-MW}}$) that are function of
121 temperature f (T), as is $\delta^{18,17}O_{MW}$ is a function of MAT (Fig. 1b), and $\Delta_{MW\text{-}WW}$ is a potential
122 evaporative offset between watershed-averaged meteoric water and weathering waters.
123 Similarly,
124

$$\Delta^{17}O_{\text{weathering product}} = \Delta^{17}O_{MW}{}^{f(T)} + \Delta_{MW\text{-}WW} + \Sigma_{i..j} (\Delta_{\text{mineral-MW}})^{f(T)} \cdot W_{i..j} \quad [3]$$

125

126 Each clay mineral, during formation and transport interacts with a variety of waters:
127 mean annual precipitation (MAP), evaporated soil waters, higher-altitude waters, diagenetic
128 waters, and finally river water, and at different environmental temperatures including mean daily
129 and seasonal climatic variations. Furthermore, some clays such as illite and chlorite may be
130 derived from recycling of older sedimentary rocks, having experienced repeated weathering
131 cycles that can reset initial O isotopic values. However, due to the large excess of meteoric water
132 involved in weathering, we argue and test below that MAT and MAP can be used as first order
133 proxies for world clay $\delta^{18}O$ signatures, yielding $\Delta^{18}O_{MW\text{-}WW} \approx 0$ in Eq. 2, thus using meteoric
134 water as the average weathering water. For $\Delta^{17}O_{WW}$ (Eq. 3), it is offset linearly from $\Delta^{17}O_{MW}$ in

a triple O space due to evaporation and mixing (Surma et al., 2018) by an increment "Excess_$^{17}O_{MW}$" discussed below.

1.3 Studied river basins and their environmental parameters (MAT, $\delta^{18}O_{MW}$)

Since Dansgaard (1964), it has become widely accepted that the mean annual $\delta^{18}O_{MW}$ of precipitation is a function of MAT (Rozanski et al., 1993; Bowen et al., 2008) (**Fig. 1b**). In this work we have compiled environmental parameters for studied river watersheds including MAT and MAP. The O and H isotopic values of corresponding watersheds and river waters were also compiled from the IAEA (Vienna) WISER dataset (https://nucleus.iaea.org/wiser/index.aspx), which contains individual publications for specific river basins (**Table A1** in the Appendix), various literature data, or as a last resort using a web-based mean annual values of waterisotopes precipitation calculator (Bowen, 2019).

When compiled $\delta^{18}O$ data for river basin waters are plotted vs MAT, linear and quadratic regressions of our dataset yield:

$$\delta^{18}O_{MW} = 0.297 \cdot MAT \cdot (°C) - 11.64; \quad R^2=0.54 \qquad [4a]$$

$$\delta^{18}O_{MW} = -0.0123 \cdot MAT^2 \cdot (°C) + 0.64 \cdot MAT - 13.05; \quad R^2=0.62 \qquad [4b]$$

The linear fit through the river water data is nearly identical to the linear fit line through global meteoric precipitation data from Bowen (2008), shifted by +0.8‰ toward heavier $\delta^{18}O_{WW}$ values, perhaps reflecting minor evaporative enrichment in soils and watersheds. This observed relationship of a positive shift in $\Delta^{18,17}O$(river water-precipitation) needs to be investigated further. The quadratic fit is also close to a quadratic approximation equation of Rozanski et al. (1993) for global precipitation data. Thus, the $\delta^{18}O$ composition of estuary and deltaic river waters closely match (±1‰) with inferred $\delta^{18}O_{MW}$ values for MAT in corresponding watersheds.

For $\delta^{17}O$, as few independent determinations of its composition is available for river and meteoric waters in watersheds, we use the global meteoric water line (GMWL) expression (Luz and Barkan, 2010):

$$\delta'^{17}O_{MW} = 0.528 \cdot \delta'^{18}O_{MW} + Excess\_^{17}O_{MW} \quad [5]$$

GMWL carries $Excess\_^{17}O_{MW}$=+0.033‰, while evaporated waters especially in soils and lakes of dry regions, have $Excess\_^{17}O_{MW} \leq 0$ (Li et al., 2015; Passey and Ji, 2019; Surma et al., 2018).

1.4 Definitions and isotope fractionations

Considering the large range of $\delta^{18}O$ values of world river clays, we use both conventional and linearized ($\Delta'^{17}O$ and $\delta'^{18}O$) notations: $\delta'^{x}O=1000 \cdot \ln(1+\delta^{x}O \cdot 10^{-3})$ in which $\delta^{x}O$ is a conventional expression $\delta^{x}O=(\frac{^{x}R_{sample}}{^{x}R_{VSMOW}}-1)\cdot 10^{3}$, the superscript *x* designates mass 18 or 17 and R is the ratio of isotope ^{x}O to ^{16}O relative to VSMOW (Miller, 2002).

In $\delta'^{x}O$ linearized coordinates, the fractionation factor $1000\ln\alpha_{clay\text{-}water}$ is simply and strictly:

$$1000\ln\alpha^{x}_{clay\text{-}water} = 10^{3} \cdot \ln(^{x}R_{clay} / {}_{x}R_{water}) = \Delta'_{clay\text{-}water} = \delta'^{x}O_{clay} - \delta'^{x}O_{w} \quad [6]$$

A reference slope of 0.5305 was adapted from Pack and Herwartz (2014) to compute $\Delta'^{17}O$:

$$\Delta'^{17}O = \delta'^{17}O - 0.5305 \cdot \delta'^{18}O \quad [7]$$

As weathering products typically consist of several types of clays (Table **A1**, Fig. **A2**) for each studied sediment sample, we plotted $1000\ln\alpha^{18}O$ for each clay in **Fig. 2**. Chlorite and illite have the lowest, while smectites and kaolinite have the highest $1000\ln\alpha^{18}O$ clay-water

fractionations (Savin and Lee, 1988; Sheppard and Gilg, 1996; Zheng, 1993), different by 2-3‰ (**Fig. 2a**). Similar shape of the curve in the relevant environmental temperature range enables easy quantification of the fractionation factors, to account for varying individual clay proportions. Furthermore, the equation for quartz-water fractionation has also a comparable shape (**Fig. 2**). When XRD data were available (**Table A1**), we computed the weighted-average bulk clay and use it throughout the calculation (dashed line on **Fig 2a**). For samples without XRD data, we used the global-average bulk clay, and individual samples with different proportions of clays vary within ~±0.5‰ from this global average value.

The illite-water second-order polynomial equation fit in the 0-300°C range is adopted from Bindeman et al (2018) to calculate $\delta^{18}O$ fractionation factors:

$$10^3 \cdot \ln\left({}^{18}R_{illite} / {}^{18}R_{water}\right) = \frac{3.825 \cdot 10^6}{T^2} - \frac{5.66 \cdot 10^3}{T} \quad [8]$$

Indeed, this second order polynomial equation is both mathematically simple and theoretically correct (1000lnα=0, when T=∞), allowing a simple solution for T.

To further quantify both ^{18}O and ^{17}O fractionation equations for other clays we select Eq. [8] for illite as a base, and numerically added increments to 1000ln$\alpha^{18}O$ to match other clays using a single equation. Thus we multiply Eqn. [8] by a constant Q, selected to range between illite and quartz:

$$10^3 \cdot \ln\left({}^{18}R_{clay} / {}^{18}R_{water}\right) = 10^3 \cdot \ln\left({}^{18}R_{illite} / {}^{18}R_{water}\right) \cdot (Q+1) \quad [9]$$

When Q=1, the equation transforms into the Quartz-water fractionation expression of Sharp et al (2016) with $1/T^2$ and $1/T$ fit coefficients of $4.28 \cdot 10^6$ and $3.25 \cdot 10^3$. Typical Q values of 0.04 to 0.08 closely reproduce the bulk clay and kaolinite-water fractionations shown in **Fig. 2.**

Likewise, for $\delta^{17}O$ and related parameter $\Delta'^{17}O$ [Eq.7], we use the illite-water fractionation from

$$\Delta'^{17}O_{\text{illite-water}} = \left(\frac{3.97\cdot10^{6}}{T^{2}} - \frac{4.9\cdot10^{3}}{T}\right)\left(0.5305 - \frac{s}{T} - \lambda\right) \quad [10]$$

where λ refers to the GMWL slope (taken as 0.528, Eq. 5). The fit parameter *s* determines the slope of the $\Delta'^{17}O_{\text{clay-water}}$ vs. $\delta^{18}O$ relationship (as illustrated later in Fig. 7). It is 1.85 for quartz-water fractionation (Sharp et al., 2016), for clay(mica)-water fractionation there are no experimental or empirical data, and we choose to vary *s* from 1.85 to 2.4 below. The rationale for this methodology is that coexisting quartz and micas precipitating from the same and common equilibrium water should maintain a slope of triple-oxygen fractionations ($\delta'^{17}O$ vs $\delta'^{18}O$) between 0.524 to 0.528 (Bao et al., 2016; Hayles et al., 2018), at relevant environmental temperatures. For example, in the temperature range 0 to 30°C and at *s*=1.85 (quartz), the average slope of $\delta'^{17}O$ vs $\delta'^{18}O$ is 0.5265, while for *s*=2.05 (mica) it is 0.5258. We used the above equations to invert measured $\delta^{18}O$, $\delta^{17}O$, and $\Delta^{17}O$ values into the $\delta^{18}O_{\text{weathering\_water}}$ and T values below.

2. Methods

2.1 Sample collection and preparation

The studied sediment samples (**Table A1**) include some of the world's largest river basins (**Fig. 1**). Smaller rivers were selected because they drain a particular context: different bedrock types i.e. volcanic provinces, old cratonic areas, sedimentary basins, or mountainous regions, and/or different climatic settings: sub-arctic, arid, wet, temperate, or tropical environments. After wet-sieving at 63µm, all sediments were sequentially leached using acetic acid, hydroxylamine hydrochloride, and hydrogen peroxide solutions to remove any carbonates, Fe-Mn oxides, and organic matter, respectively (Bayon et al.,2002, 2015). Residual clay- (<4µm, with most particles <2µm), silt- (4-63µm), and sand- (~63-100µm) size fractions were then separated by centrifugation. The sands selected were from the Mississippi, Yangtze, Brahmaputra, Mekong, Yellow, Fraser, and Fly Rivers (**Table A2**).

227

228 **2.2. Oxygen isotope analysis.** To extract O_2 from silicate minerals, we used a CO_2-laser
229 fluorination line with BrF_5 as the reagent. For highly reactive at room-temperature clays, we
230 specially built an "airlock" sample chamber where samples are introduced and fluorinated
231 individually (Bindeman et al., 2018). For triple-oxygen isotope analysis, we further used gas
232 chromatographic and cryogenic purifications, with each extraction and analysis (>4 analyses of 8
233 cycles) taking ~1.5 hours. Silt- and sand-size detrital samples, and also several clay-size samples
234 with a limited amount of available material (<0.7 mg), were analyzed only for $\delta^{18}O$. San Carlos
235 olivine (SCO), $\delta^{18}O$=5.1 and $\Delta'^{17}O$=-0.05‰, (Pack et al., 2016), and Gore Mtn. garnet (UWG-
236 2, $\delta^{18}O$=5.75 and $\Delta'^{17}O$=-0.065‰ Miller et al., 2019) and in house garnet UOG ($\delta^{18}O$=6.52 and
237 $\Delta'^{17}O$=-0.06‰, Zakharov and Bindeman, 2019) were used as standards to normalize to the
238 VSMOW scale.

239 The $\delta^{18}O_{WIC}$ (water-in-clays), total water wt%, were determined on 0.4-0.7mg clay
240 samples by glassy-carbon pyrolysis at 1450°C using the TCEA/MAT-253 system (e.g., Seligman
241 and Bindeman, 2019). Prior to analysis the clays were dried under vacuum at 200°C for 14-24 h
242 (Gilg et al., 2004; Bauer and Vennemann, 2014), then immediately (over 3-5 min) loaded into
243 the helium atmosphere of the TCEA autosampler. Such quick transfer procedure was tested not
244 to result in atmospheric water absorption.

245

246 **3. Results**

247 **3.1. $\delta^{18}O$, $\delta^{18}O_{WIC}$ and $\Delta'^{17}O$ values of clays, silts and sands, and estimated weathering**
248 **product**

249 **Tables A1 and A2** present the large analytical dataset for world rivers that we assembled
250 herein, including triple-oxygen isotopic values for clays, $\delta^{18}O_{WIC}$ (water-in-clays), total water by
251 TCEA, $\delta^{18}O$ values of silt- and sand size fractions from the same samples, and $\delta^{18}O$ values for
252 detrital sands from seven major river systems.

253 Here we use XRD data-determined identities and proportions of bulk clays (**Fig. A2,A3**)
254 to compute theoretical equilibrium $\delta^{18}O$ and $\delta^{17}O$ values for clays formed with the MAT and
255 $\delta^{18}O_{MW}$ characteristics of corresponding watersheds (**Fig. 2),** using fractionation factors for
256 individual clays (e.g. Eq. 2-3). The average "bulk clay" shown in Fig. 2a consists of 34%
257 smectite, 22% kaolinite, 29% illite, and 15% chlorite.
258 The majority of studied fine-grained river sediments show high-$\delta^{18}O$ values as expected
259 for weathering products. However, it is important to determine what proportion of their mass can
260 be derived from recycling of older and similarly high-$\delta^{18}O$ authigenic weathering components
261 (e.g. flaky overgrowth quartz skins), or low-$\delta^{18}O$ igneous and metamorphic detritus that
262 underwent only physical erosion and grain size reduction, without chemical alteration. This issue
263 was evaluated using: i) the chemical index of alteration (CIA, using XRF data from Bayon et al.
264 2015, 2018) that can be used to estimate the proportion of unweathered mica and feldspar with
265 CIA=50, and ii) the total measured water content of the clay and silt samples, that provide
266 estimates for anhydrous detrital mineral contribution (e.g. feldspars, quartz, **Table A1**, **Fig. 3,**
267 **A4**). Clay samples show scatter and no trends with CIA, while silts have smaller CIA and more
268 detrital, and water-poorer compositions (**Fig. 3**).
269 Two mass balance equations are solved to obtain the O isotopic composition of the
270 authigenic fraction of a sediment sample that we refer to as 'weathering product', $\delta^{18}O_{WP}$. For
271 the CIA-based approach we use:
272
273 $$x \cdot \delta^{18}O_{detrital} + (1-x)\ \delta^{18}O_{wp} = \delta^{18}O_{bulk}, \text{ where } x = (CIA-50)/(90-50) \quad [11]$$
274 and the fully-weathered, authigenic component is assigned a CIA value appropriate for their
275 XRD-determined clay mineralogy where available, or the global average bulk clay composition,
276 with a typical CIA=90. The $\delta^{18}O$ and $\Delta'^{17}O$ values of the detrital component are taken as 11.5‰
277 and -0.108‰ respectively, with CIA=50 and 1.8wt% H_2O as is estimated below.
278 For the water-based approach we use:
279

$$y \cdot \delta^{18}O_{detrital} + (1-y)\ \delta^{18}O_{wp} = \delta^{18}O_{bulk}, \text{ where } y = (Z - H_2O)/Z \quad [12]$$

where H_2O is measured water, and Z is computed stoichiometric H_2O in the bulk clay for each sample; average bulk clay has 10.1wt% H_2O. Identical mass balance equations are independently written for $\Delta^{17}O$ and all equations are solved for $\delta^{18}O_{WP}$ and $\Delta^{17}O_{WP}$. Note that mixing lines are linear in unprimed $\delta^{18}O$ and $\Delta^{17}O$ notation and are used for these calculations.

Measured mineralogical proportions of individual clays determined by XRD (Bayon et al., 2015, 2016, 2018; **Table A1**) permit independent estimation of theoretical CIA and water content for each sample, as different clays show variable H_2O and CIA. For example, stoichiometric kaolinite has CIA=100 and 14wt% H_2O, while illite has CIA=85 and 6wt% H_2O. Kaolinite-rich samples with more than 12.5wt% water on average, and CIA>90 have x and y values that are slightly greater than 1, and are assumed here to be fully authigenic with x=y=1.

Below we use both of these estimates of detrital wt% and compute the theoretical isotopic values of weathering products in **Table A1 and Fig. 6**, and we choose to use their average when both are available. Note that these two independent detrital indices provide semi-quantitative estimates for detrital contribution. In order to make them fully quantitative, both the chemistry and stoichiometry of each of the contributing clay mineral phases should be known.

We observe that most clay-rich samples that we analyzed are dominated by weathering products (**Table A1, Fig. 3-6, A4**). XRD spectra (**Fig. A5**) identify the presence of a few detrital minerals (quartz, feldspar, amphibole) with peak areas being proportional to the individually assessed detrital proportion based on CIA and/or water content (**Table A1**). Additionally, the low CIA in clay-rich samples containing only small identifiable amounts of feldspars and biotites, could result from the presence of chemically-immature and recycled older clays such as illite and some smectite, with low-CIA and low-H_2O (Newman, 1987). Detrital proportions were used to compute $\delta^{18}O_{WP}$ and $\Delta^{17}O_{WP}$ compositions of weathering products; these likely provide maximum estimates, with values for true weathering products lying somewhere in between these and raw measured clay values, given the uncertainty of individual clay chemistry (Sheppard and Gilg, 1996).

3.2. Lack of bedrock compositional influence on clay $\delta^{18}O$ values

One important pre-requisite is to test whether the observed $\delta^{18}O$ variations in studied samples could relate (at least partially) to differences in the mean $\delta^{18}O$ lithological composition of their watersheds. In this study, we observe no significant $\delta^{18}O$ difference in clays derived from contrasted geological settings and draining different bedrock types (**Fig. 1, A2; Table A1**). For example, studied river basins in Ireland, which are characterized by nearly identical MAT and $\delta^{18}O_{MW}$ but drain contrasted lithologies, confirm this test well (**Table A1, Fig A2**). Blackwater and drain high-$\delta^{18}O$ Paleozoic sedimentary formations (with an assumed bulk rock composition of +12 to +16‰), while Foyle River drain Proterozoic metamorphic rocks (+10 to +13‰), and Six-Mile and River Maine drain Tertiary volcanic rocks (+6‰), respectively. However, for each of these rivers, measured $\delta^{18}O$ clay values are higher than corresponding bedrock compositions, all exhibiting a similar range of +16-18‰ values indicating equilibrium with meteoritic waters at MAT and $\delta^{18}O_{MW}$ of Ireland. Similar observations characterize our global dataset, where bedrock types are estimated using the Global Lithological Maps (GLiM) database of Hartmann and Moosdorf (2012), including the largest world rivers with comparable climates, such as Congo (50% metamorphic basement, $\delta^{18}O_{clay}$=19.0‰), Amazon (75% sedimentary basement, $\delta^{18}O_{clay}$=17.7‰), and Niger (45% metamorphic, $\delta^{18}O_{clay}$=18.0‰), suggesting clearly that protolith composition does not play an important role in controlling the O isotopic composition of studied fine-grained sediments. Therefore, the composition of regional meteoric waters $\delta^{18}O_{MW}$ and the mean annual temperature of watersheds (**Fig. 1-2**) most likely represent the two dominant factors influencing $\delta^{18}O$ of the fine sediment fractions transported by river systems. The $\delta^{18}O$ exhibits no correlation with $\delta^{30}Si$ for the same samples (**Table A2**).

Sand-size fractions from seven major world rivers, which potentially represent the $\delta^{18}O$ composition of the eroding continents, range between 9.6 and 12.9‰ (**Table A2**), and average 11.4±1.1‰ (**Table 1).**

3.3. Correlations with Mean Annual Temperature (MAT) and clay-water fractionation factors

Figures 4-6 present variations in $\delta^{18}O_{bulk\_clay}$, $\delta^{18}O_{WIC}$, $\delta^{18}O_{WP}$, and $\Delta'^{17}O$ with MAT and $\delta^{18}O_{MW}$. A notable feature is that neither the $\delta^{18}O_{bulk\_clay}$ nor $\delta^{18}O_{WIC}$ show global correlation with MAT (**Fig. 4**), despite the fact that studied river basins encompass a large range of climatic conditions, from Arctic to equatorial regions (**Fig. 1**). The $\delta^{18}O$ composition of silt-size fractions largely overlaps with clays at T>15°C. This suggests that under warm conditions both silts and clays result from thoroughly weathered materials. Studied silts contain less clay and water (typically ~3wt%, **Fig. 3, A4**), and are represented by isometric and mostly translucent and birefringent particles under the microscope, suggesting that their high $\delta^{18}O$ value must be inherited from the presence of weathering-related silica and albite, but not from detrital igneous and metamorphic quartz and feldspars (with lower $\delta^{18}O$). A scattered positive correlation for silts with MAT (**Fig. A4**) suggests first order climate control on their stable isotopic composition, and tropical silts contain more water due to kaolinite (**Fig. A3**). There is no apparent global correlation of $\delta^{18}O$ clay or silt with the amount of mean annual precipitation (MAP) or river discharge for studied rivers (not shown).

In contrast, **Figure 5** presents computed isotope fractionations between clays and the meteoric water that was involved in weathering in their respective watershed areas, showing strong positive correlation with MAT. As expected, increasing temperature causes a decrease in clay-water isotope fractionation (**Fig. 1a**) and this is precisely what is observed in our global dataset. We computed the bulk-clay water isotope fractionation for each sample and observe a subparallel trend with the best-fit line for natural data. The ~2‰ offset for equilibrium vs measured clay $\delta^{18}O$ is explained by admixture of lower $\delta^{18}O$ detrital materials, or immature and inherited clays, to each of the samples, as is documented in Fig. **A3** and described above. Similarly, mirror image, clay-water isotope fractionation relationships are observed for $\Delta'^{17}O$ (**Fig. 5b**).

359 This work also presents a rarely reported dataset for water-in-clay, $\delta^{18}O_{WIC}$. We observe
360 that $\delta^{18}O_{WIC}$ values and their fractionation with local meteoric waters remains constant despite
361 variation in MAT, and interestingly, also shows subparallel correlation to $\delta^{18}O_{bulk\_clay}$. In this
362 study, we calculate an average $\delta^{18}O_{bulk\_clay}$ - $\delta^{18}O_{WIC}$ fractionation offset of 7.9±3.3‰ (1stdev of
363 the mean), together with a computed average $\delta^{18}O_{silicate}$ - $\delta^{18}O_{WIC}$ fractionation of 9.2±3.3‰ by
364 mass balance. There is minimal change in $\Delta^{18}O=(\delta^{18}O_{bulk\_clay}- \delta^{18}O_{WIC})$ with increasing MAT
365 based on linear fit parameters, within the 1-2‰ error in these measurement. Intra-mica, water-
366 silicate isotope fractionation has not been studied in sufficient detail, and a highly diverse set of
367 fractionation factors, between 5 and 14‰ is predicted for various phyllosilicates (muscovite and
368 kaolinite, Hamza and Epstein, 1980; Bechtel and Hoernes, 1992; Zheng, 1993a; Seligman and
369 Bindeman, 2019). Water-in-mica $\delta^{18}O$ isotopic fractionations are likely to be controlled by clay
370 chemistry, mostly variation in wt% Fe content, and H_2O to OH proportions as much as
371 temperature (Sheppard and Gilg, 1996). Nonetheless, our observation here that $\Delta^{18}O_{bulk\_clay\text{-}WIC}$
372 stays within a 7-9‰ range between bulk clay and its water across the world's varied climates,
373 and limited change with MAT, provides an important empirical observation to the question of
374 isotopic fractionation between clays and their water.
375 Overall, our new global average $\delta^{18}O_{WIC}$ value of +8.1±1.9‰ (**Table 1**), is higher than
376 the +5.5‰ mantle. This suggests that the 10-12‰ water released from sedimentary clays during
377 subduction always carries a positive, rather than negative $\delta^{18}O$ signal. However, most of
378 subduction water released is likely from high-temperature hydrothermal clays with lower than
379 mantle $\delta^{18}O_{WIC}$ values.
380 The computed $\delta^{18}O_{WP}$ and $\Delta'^{17}O_{WP}$ isotopic compositions of the weathering product
381 associated with each studied clay sample after correction for dilution by primary detrital minerals
382 (Eqs. 11-12) are also plotted in **Fig. 6,** and they exhibit no correlation with MAT, or slightly
383 parabolic. This is explained by the counterbalancing effects of $\delta^{18}O_{MW}$ and isotopic fractionation
384 with temperature (**Fig. 1b and 2a**).
385

3.4. Triple oxygen isotope insights into weathering

The measured triple-oxygen isotopic values for clays are plotted in a $\delta^{18}O$-$\Delta'^{17}O$ diagram (**Fig. 7**) to investigate the independent effects of temperature and $\delta^{18}O_{MW}$ of parental meteoric waters on the isotopic values of clays (e.g. Bindeman et al., 2018). When our dataset is split into three 'climate' zones: tropical, temperate, and arctic climates (according to MAT, **Fig. 7**), there is significant overlap between studied samples. This finding agrees with what was reported above when considering the lack of correlation between $\delta^{18}O$ and $\Delta'^{17}O$ versus MAT (**Fig. 6**), but in **Fig. 7**, these two parameters have their own dependence on temperature (**Eq. 9-10**). Another interesting observation is that modern clays from major world rivers overlap with the range of values previously measured for Phanerozoic and post-2.2 Ga Proterozoic shales, while Archean shales that are shown for comparison display lower isotopic diversity of water and overall higher T.

Global average values for $\delta^{18}O$ and $\Delta'^{17}O$ in bulk clays and weathering products are given in **Table 2**. Tropical clays are characterized by mean $\delta^{18}O$ and $\Delta'^{17}O$ values of 16.31‰ and -0.136‰, respectively (derived from a mean $\delta^{18}O_{MW}$ of -5.37‰ and 25.7°C temperature. In contrast, subarctic river basin clays (with average MAT of 1.2°C and $\delta^{18}O_{MW}$= -13.4‰) have $\delta^{18}O$ and $\Delta'^{17}O$ values of 14.52‰ and -0.153‰ respectively. Triple-oxygen isotopic values for temperate and subtropical environments fall between these end member values. Such a small overall range is a reflection of strong counterbalancing effects of decreasing isotope fractionations (Eqs. 2,3) with increasing MAT and decreasing $\delta^{18}O_{MW}$ ($\Delta'^{17}O_{MW}$) with increasing MAT (Eq. 4, **Fig. 1, A1**). The remarkable lack of correlation of bulk world river clays from markedly different climatic regions is unfortunate news for isotope climatology, while regional and monomineralic clay studies (Sheppard and Gilg, 1996) are still robust. The absence of correlation enables us to calculate a global average triple-oxygen isotopic value for bulk clay that is relevant for computing balances among different geochemical reservoirs (Muehlenbachs and Clayton, 1976; Holland, 1984; Muehlenbachs, 1998; Sengupta and Pack, 2018). Below, we compute global weathering fluxes using $\delta^{18}O$ and $\Delta'^{17}O$ in total suspended sediment

(TSS=clay+silt) flux supplied by rivers from different climates, and weight them by the amount of sediment for each continental region (**Table 2**).

4. DISCUSSION

Our dataset for $\delta^{18}O$ and $\Delta'^{17}O$ in clays and silts and comparison with computed theoretical estimates for expected values of equilibrium fractionations, provides further evidence that measured clay- and silt- size fractions are representative of the average weathering product derived from their respective watersheds and climatic setting, with only minor contribution from primary detrital and/or recycled and post-diagenetic clay minerals. These results are best explained by the progression of chemical weathering by silicate hydrolysis reactions (Eq. 1) at very high water/rock ratios, which results in effective oxygen isotopic exchange with local meteoric waters having $\delta^{18}O$ composition and temperature similar to basin-scale regional estimates (**Fig. 1**). Lack of $\delta^{30}Si$ and $\delta^{18}O$ correlation for the same samples suggest that silicon isotopes are partly controlled by the bedrock (**Table A1**).

4.1 Inverting measured $\delta^{18}O$ and $\Delta^{17}O$ clay values to $\delta^{18}O_{WW}$ and T of weathering.

Our triple-oxygen dataset enables independent determination of temperature, and $\delta^{18}O$ of parental weathering water. The measured $\delta^{18}O_{clay}$ and $\delta^{17}O_{clay}$ values, and the weathering-meteoric water line equation [5], are used as input parameters to invert the system of fractionation equations [9]-[10] to solve for three unknowns (T, $\delta^{18}O_{MW}$ and $\delta^{17}O_{MW}$). We used a similar approach in our earlier study of modern and ancient shales (Bindeman et al., 2018).

We then compare computed weathering water compositions and temperature with observed watershed meteoric water and temperature in **Fig. 8**, and make the following observations.

i) Using measured $\delta'^{18}O$ and $\Delta'^{17}O$ ($\delta'^{17}O$) values of clays as input parameters (**Fig. A6**), without correcting for detrital contributions, the computed range of temperatures and $\delta^{18}O_{WW}$

overlaps within ~10°C and 4‰ $\delta^{18}O_{MW}$ with observed values, although some computed temperatures are unrealistically high, >45°C. ii) Likewise, the computed $\delta^{18}O_{WW}$-T relationship matches the global $\delta^{18}O_{MW}$-MAT (**Fig. 1b**) slope but with an offset. iii) When $\delta'^{18}O_{WP}$ and $\Delta'^{17}O_{WP}$ of the weathering products are used as input parameters instead, and by using weathering water with "Excess_$^{17}O_{MW}$ "=0 to -0.03‰ (Eq. 5), the match of computed and observed values is better, resulting in nearly complete overlap (**Fig. 8**).

Sensitivity analysis of the final output in $\delta^{18}O$-T relationship was performed by varying parameters in the input eqns. [5], [8]-[10] above, by 1) increasing the slope *s* of the triple-oxygen $\Delta^{17}O$ vs $\delta^{18}O$ relationship (see **Fig. 7** inset for explanation) from 1.85 to 2.4 as per equation [10], 2) changing the "Excess_$^{17}O_{MW}$" from +0.033 to -0.05 as per Equation 5 from Global MWL, (+0.033, Luz and Barkan, 2010) to zero, and more negative values being characteristic of strongly evaporated and mixed waters (Herwartz et al., 2017), or 3) varying the 0.528 slope of the MWL in the range 0.527-0.530.

The best overlapping solution was found by keeping the MWL slope of 0.528 as suggested by Luz and Barkan (2010), but with "Excess_$^{17}O_{MW}$"=0, by using the CIA- or water-corrected weathering product rather than those of the raw clay; by using the slope *s* (fit coefficient in Eq [10]) between 1.85 and 2.05 (**Fig. 7, 8 and A6**).

In summary, our modeling exercise of using triple-oxygen isotope values of clays from modern river basins data to compute weathering parameters T and $\delta^{18}O_{WW}$, provides further evidence that these clays broadly reflect the average weathering conditions (T and $\delta^{18}O_{MW}$) in their watersheds. This "zero"-test hypothesis also implies that applying the triple-oxygen isotopic composition of clays to resolve T and $\delta^{18}O_{WW}$ in ancient environments, as in Bindeman et al. (2018), is possible and justified by modern samples. The affirmation of the 0.528 slope of the GMWL in modern and Archean hydrosphere as a preferred solution and a robust result. The better fit of our dataset by using weathering water line parallel to the GMWL (Fig. 7) but without the ^{17}O excess parameter of +0.033 needs better explanation. First, the value of this offset (which is analogous to the deuterium excess =10 in the meteoric water relation $\delta D_{MW}=8\cdot\delta^{18}O_{MW}+10$) is

466 debated within the hydrological community (Cappa et al., 2004; Uemura et al., 2010; Li et
467 al., 2015). Second, soil water evaporation effects and rain-soil water mixing processes lead to
468 excess in $\delta^{18}O$ and deficiencies in 17-O, especially in dry tropical and subtropical environments
469 (Hsieh et al., 1998; Herwartz et al., 2017; Passey and Ji, 2019). The latter possibility is
470 intriguing for our clay dataset, requiring new targeted studies, and may suggest that weathering
471 in watersheds, especially arid, proceeds with slightly evaporated and mixed waters. However, by
472 comparing real $\delta^{18}O_{MW}$ and computed $\delta^{18}O_{WW}$ values, they return either similar or lower (not
473 higher) $\delta^{18}O_{MW}$ values that would be characteristic for strongly evaporated waters. This suggests
474 minimal effects of evaporation on $\delta^{18}O_{WW}$, and that weathering proceeds by great excess of
475 diverse watershed meteoric waters appropriate for watersheds rather than soil waters highly
476 enriched in $\delta^{18}O$.

477 **4.2 Estimating $\delta^{18}O$ and $\Delta^{17}O$ of average exposed crust undergoing weathering**

478 We presented examples in section 3.2 that the lithology did not play a major role in
479 controlling the $\delta^{18}O$ composition of resulting weathered products. A global $\delta^{18}O$ estimate for the
480 average exposed crust undergoing weathering is required to calculate weathering fluxes, i.e.
481 $\delta^{18}O_{clay+silt}$ -$\delta^{18}O_{crust}$ and $\Delta^{17}O_{clay+silt}$ -$\Delta^{17}O_{crust}$ into the hydrosphere (**Tables 1-2**). We address this
482 issue by using five independent methods.

483 First, our average value for the sand fractions derived from seven major world rivers
484 (Mississippi, Yangtze, Brahmaputra, Mekong, Fraser, Fly, and Yellow Rivers) is
485 $\delta^{18}O$=11.38±1.18. Studied detrital sand fractions are mostly source rock unweathered primary
486 minerals, and thus are well suited for estimating the average composition of the eroded crust
487 undergoing weathering. A composite sample of these sands yields +11.98‰ and $\Delta'^{17}O$ = -
488 0.101‰ (Table 1).

489 This can be validated using a second approach in which the observed $\delta^{18}O$ vs. CIA (**Fig.**
490 **3**) and CIA vs. H_2O relationships (**Fig. A4a**) for silts are used to derive a hypothetical detrital
491 end-member at CIA=50, with $\delta^{18}O$=11.5‰ and 1.8wt% H_2O. The latter, suggests that the
492 projected global detrital component is not fully anhydrous, as it likely contains igneous biotites

493 (CIA=50, 3.5wt% water) and ordered micas such as muscovite and illite from post-diagenetic
494 sedimentary and metamorphic rocks.
495 Third, by using the Global Lithological Map of the world database (Hartmann and
496 Moosdorf, 2012), we assigned $\delta^{18}O$ values to exposed surface rocks on continents normalized to
497 their estimated areas of exposure (**Table 1**). Such an integrative approach yields $\delta^{18}O$=+11.83‰
498 and $\Delta'^{17}O$=-0.108‰ ($\Delta^{17}O$=-0.125‰) for modern silicate surfaces exposed to weathering.
499 Varying proportions of rock types by ±10% and their $\delta^{18}O$ values by ±1‰ in a Monte-Carlo
500 simulator carries a ±0.6‰ standard deviation to this estimate.
501 Fourth, the $\delta^{18}O$ composition of glacial tillites worldwide (Gaschnig et al., 2016;
502 Bindeman et al., 2016), evaluates the average $\delta^{18}O$ of glacially-eroded and regionally-averaged
503 portions of continental crust at +11.5±2.9‰ (n=75).
504 Fifth, our unpublished triple-oxygen isotope dataset for global ignimbrites from actively
505 deforming areas averages +8.5‰±2‰. Ignimbrites represent a blend among high in $\delta^{18}O$ but
506 diverse continental crust types, sampling mostly isotopically diverse upper and middle crust, and
507 mantle-like basaltic differentiates ($\delta^{18}O$ and $\Delta'^{17}O$ values of +5.7 and -0.05‰). When
508 independently corrected for the relative amounts of mantle using linear mantle-crust mixing
509 equations mathematically similar to Eqns. [11] and [12], but by employing the "Nd-isotope
510 crustal index" of DePaolo et al. (1992), we estimate the $\delta^{18}O$ and $\Delta'^{17}O$ values of upper crust as
511 +10±2‰ and -0.1‰.
512 Average of five methods above gives an estimate of $\delta^{18}O$=11.3±0.7‰. Based on first two
513 approaches, we propose $\delta^{18}O$=+11.5‰ and $\Delta'^{17}O$ =-0.108‰ as the average values for the
514 exposed crust undergoing weathering. We assign respective arbitrary ~1‰ and 0.01‰ standard
515 deviations to this estimate, in order to account for observed differences among river basins and
516 other uncertainties.
517 An important observation is that the weathering products TSS (clays+silts) from nearly
518 all studied major river basins except Brahmaputra, show a positive $\delta^{18}O$ shift compared to the
519 $\delta^{18}O$ value for the exposed continental crust from which it was derived, and thus carrying

520 negatively-shifted $\delta^{18}O$, and positively-shifted $\Delta'^{17}O$, water fluxing into the hydrosphere. In
521 contrast, river bedloads represented by sands with $\delta^{18}O$ values at +11.38‰, are almost identical
522 to the estimated exposed continental crust average of +11.5‰ (Table 1), suggesting that coarser
523 products transported by rivers carry zero $\Delta(\delta^{18}O)$ weathering flux.
524
525 **4.3 Reassessing global weathering flux to the modern and Quaternary hydrosphere**
526 Table 2 presents globally-averaged continental silicate weathering fluxes, computed as
527 TSS minus bedrock global O isotopic values, yielding: $\Delta\delta^{18}O$=-2.59±0.38‰ and $\Delta\Delta'^{17}O$ =
528 +0.043±0.0065‰ for the modern Earth. For the largest river basins we also used the GLiM
529 database to compute watershed-averaged $\delta^{18}O$ values based on proportions of exposed rock
530 types, but the final estimate carries little difference as compared to just using the global average
531 $\delta^{18}O$ bedrock value of +11.5‰. Our new silicate weathering flux estimate is 50% higher than
532 previous and currently accepted weathering advance estimate of $\Delta\delta^{18}O$=-1.8‰ (Holland, 1984;
533 Muehlenbachs, 1998).
534 Continental weathering flux must also include fluxes from weathering limestones,
535 constituting 7.9% of surface area (Hartmann and Moosdorf, 2012). These are more difficult to
536 estimate as carbonate ^{18}O and ^{17}O weathering fluxes depend on the assumed average $\delta^{18}O$ and
537 $\Delta'^{17}O$ values of marine carbonate exposed to low-$\delta^{18}O$ rain or karst solution-reprecipitation. At a
538 20.3°C, and $\delta^{18}O_{MW}$= -7.3‰, globally averaged, sediment-fluxed weighted, weathering
539 conditions estimated here (**Table 2**), a carbonate with +21.5‰ relative to SMOW will be in
540 equilibrium with the modern hydrosphere, leading to zero net ^{18}O and ^{17}O fluxes. However,
541 weathering of an average marine Phanerozoic limestone with +25.8‰ as in Simon and Lecuyer
542 (2005), will release additional ^{18}O, and reduce the flux-weighted global negative $\delta^{18}O$ flux from
543 silicate weathering to the hydrosphere by a maximum 0.3‰, thus diminishing newly-estimated
544 total weathering advance from -2.59 to -2.24‰. Weathering of metamorphic carbonates (e.g.
545 marble of +14‰, Simon and Lecuyer, 2005), will diminish the sedimentary carbonate
546 contribution.

547 Using the 19.1Gt/yr global suspended sediment flux (TSS=clay+silt) to the ocean of
548 Milliman (2011), which is surprisingly consistent with the earlier estimate of 20 Gt/yr of Holland
549 (1984) and Muehlenbachs (1998), based on Holeman (1968), we can calculate the modern
550 global $\delta^{18}O$ flux using the following equation:

551 $$-2.59‰ \cdot 19.1\text{Gt/yr} \cdot 0.5 = 25(\pm 3.6)\text{Gt}\cdot‰/\text{yr of Oxygen-18} \quad [13]$$

552 where 0.5 is fraction of O in the rock.

553 The reasons for our upward revision of global ^{18}O flux given in **Table 2**, are due to
554 recent reassessment of regional river sediment fluxes (Milliman and Farnsworth, 2011)
555 suggesting that about 2/3 of the global TSS flux occurs in SE Asia and western Pacific regions
556 (Table 2). Active tectonics and intense rainfall events in SE Asia and western Pacific, together
557 with a greater proportion of igneous and commonly lower-$\delta^{18}O$ (higher-$\Delta^{17}O$) basaltic rocks such
558 as volcanic edifices and batholiths yield greater weathering advance $\Delta\delta^{18}O$ over bedrock.
559 Additionally, previous researchers followed Holeman's (1968) assessment that 75% of the TSS
560 in rivers corresponded to recycled sediment with a somewhat arbitrarily assigned $\delta^{18}O$ =+17‰,
561 while the remaining 25% were split equally between igneous (+7‰) and metamorphic (12‰)
562 rocks. Our estimates (Tables 1 and 2) are based on real measurements and exposed sediment
563 proportion in GLiM database.

564 We write the equation in general terms with the aim to mass-balance modern world and
565 seawater $\delta^{18}O$ and $\delta^{17}O$ values and apply it to the past hydrosphere:

566
567
$$m_{Oc}\frac{d}{dt}(\delta^{17,18}O_{Oc}^{(t)}) + \delta^{17,18}O_{Oc}\frac{d}{dt}(m_{Oc}^{(t)}) = \sum_{1}^{j} F_j \cdot \Delta(\delta^{17,18}O)_j + F_{mr}^{(t)} \cdot \Delta(\delta^{17,18}O)_{mr}$$
568

569 With F_j fluxes to include: high- and low-T submarine alteration, continental growth,
570 water recycling, and continental weathering (Muehlenbachs,_1998; Table A3). The F_{mr}(t) is
571 mantle rehydration term related to irreversible loss of water (and ocean level drop), due to

572 hydrous slab subduction to the deep mantle (e.g., Parai and Mukhopadhyay, 2012) by plate
573 tectonics, modulated by supercontinent cycle. This predominant loss is likely of low-$\delta^{18}O$
574 serpentinized interior of slabs, leading to temporally positive $\delta^{18}O$ shifts of ocean. We allow for
575 mass of ocean and its $\delta^{17,18}O$ values to change. However, for most recent timescale (or constant
576 m_{Oc} and $\delta^{17,18}O_{Oc}$) the LHS of the equation is 0, giving a conventional steady state ocean isotopic
577 mass balance of Holland (1984) and Muehlenbachs (1998).
578 Thus, for present and Late Cenozoic world, our estimated 50% higher continental
579 weathering flux, which removes ^{18}O and ^{17}O from the oceans, yields the $\delta^{18}O$, $\delta^{17}O$, and $\Delta^{17}O$ of
580 the current hydrosphere as -0.784‰, -0.4328‰ and -0.0168‰ respectively (Table A3). Within
581 error, this value agrees with the target $\delta^{18}O$ ocean estimate of -1‰ for ice-free world (Shackleton
582 and Kennett, 1975). Our new estimate also allows to constrain the main counterbalancing and
583 elusive flux - high-T hydrothermal alteration at mid-ocean ridges (correlating to plate tectonics
584 spreading rates) that leaches ^{18}O and ^{17}O from the rocks into the oceans. It need to be only 10%
585 lower of its current estimate to sustain $\delta^{18}O$=-1‰ ice-free ocean.
586
587 **5. Conclusions**
588 1) Oxygen isotopes in the fine-grained clay-rich sediments from world rivers primarily
589 record the isotopic composition of regional precipitation, offset by appropriate fractionation
590 factors, rather than the O isotopic composition of underlying bedrocks. This is explained by high
591 water/rock ratios during weathering.
592 2) The global sediment flux-weighted $\delta^{18}O_{MW}$ responsible for weathering is -7.3‰, with
593 most global weathering proceeding at 20.3°C.
594 3) Modern bulk clays do not vary much isotopically between different climatic zones
595 worldwide, a simple relationship explained by opposing effects of temperature on clay-water
596 fractionation and on $\delta^{18}O_{MW}$.
597 4) Mathematical inversion of measured clay $\delta^{18}O$ and $\Delta'^{17}O$ values into temperature and
598 $\delta^{18}O_{WW}$, using appropriate fractionation factors and estimates of detrital dilution, returns

599 satisfactory results when compared to observed mean annual temperatures (MAT) and $\delta^{18}O_{MW}$ in
600 each studied river basin.
601 5) The global $\delta^{18}O$ and $\Delta^{17}O$ average compositions of the fine-grained sediment (TSS)
602 exported to the ocean, after normalization to regional sediment fluxes, are +14.09‰ and
603 $\Delta^{17}O$=-0.164‰, while the exposed continental crust undergoing weathering is estimated to be
604 +11.5‰ and $\Delta'^{17}O$=-0.108‰ ($\Delta^{17}O$=-0.125‰) (Table 1).
605 6) Total $\delta^{18}O$ and $\Delta^{17}O$ weathering flux into the oceans due to silicate weathering is
606 -2.59±0.38‰ and +0.0432±0.0065‰ respectively. This $\delta^{18}O$ flux is 50% higher the previous
607 estimate, suggesting that weathering is more efficient in removing ^{18}O from the hydrosphere.
608 7) Our new estimate when used in the global O isotope flux models of Muehlenbachs
609 (1998), and Sengupta and Pack (2018), supports values of $\delta^{18}O$= -0.78‰ and $\Delta^{17}O$= -0.0168‰
610 for ice-free oceans, close to the expected $\delta^{18}O$ value of -1‰, and suggesting that global long-
611 term O isotopic budgets and estimated counterbalancing fluxes are accurate and are adding up.
612 8) Observed increase in $\delta^{18}O$ and stepwise decrease in $\Delta^{17}O$ in shales in the geologic
613 record may thus capture: i) evolving global hydrologic cycle upon continental emergence of large
614 subaerial continental land masses, ii) decrease in global MAT, and iii) decreasing mass of ocean
615 due to irreversible rehydration of the mantle via subduction of hydrous low-$\delta^{18}O$, high-$\Delta^{17}O$
616 slabs.
617

618 **Acknowledgements.** The funding is provided by NSF grants #1833420 and 1822977
619 the University of Oregon, and the Swiss NSF (grant # IZSEZ0_180188). We thank Daniel
620 Herwartz for his careful detailed review, anonymous reviewer, and Frederic Moynier, Nick
621 Greber, David Zakharov and Albert Gilg for comments.
622
623 **REFERENCES**

624 Bao, H. M., Cao, X.B., Hayles, J., 2016. Triple-oxygen isotopes: fundamental relationships and
625 applications. Annu. Rev. Earth Planet. Sci. 44, 463–492.

626 Bauer, K., Vennemann, T., 2014. Analytical methods for the measurement of hydrogen isotope
627 composition and water content in clay minerals by TC/EA. Chemical Geology 363, 229–240.
628 DOI: 10.1016/j.chemgeo.2013.10.039
629 Bayon, G., Delvigne, C., Ponzevera, E., Borges, A.V., Darchambeau, F., De Deckker, P.,
630 Lambert, T., Monin, L., Toucanne, S., André L., 2018. The silicon isotopic composition of
631 fine-grained river sediments and its relation to climate and lithology. Geochim. Cosmochim.
632 Acta 229, 147-161.
633 Bayon, G., Skonieczny, C., Delvigne, C., Toucanne, S., Bermell, S., Ponzevera, E., André L.,
634 2016. Environmental Hf–Nd isotopic decoupling in World river clays. Earth Planet. Sci. Lett.
635 438, 25-36.
636 Bayon, G., Toucanne, S., Skonieczny, C., André, L., Bermell, S., Cheron, S., Dennielou, B.,
637 Etoubleau, J., Freslon, N., Gauchery, T., Germain, Y., Jorry, S.J., Ménot, G., Monin, L.,
638 Ponzevera, E., Rouget, M.-L., Tachikawa, K., Barrat, J.A., 2015. Rare Earth elements and
639 neodymium isotopes in World river sediments revisited. Geochim. Cosmochim. Acta 170,
640 17–38.
641 Bechtel, A., Hoernes, S., 1990. Oxygen isotope fractionation between oxygen of different sites in
642 illite minerals: A potential single-mineral thermometer. Contrib. Mineral. Petrol. 104, 463–
643 470.
644 Bindeman, I.N., Zakharov, D.O, Palandri, J., Greber, N.D., Retallack, G.J., Hoffman, A.,
645 Dauphas, N., Lackey, J.S., Bekker, A., 2018. Rapid growth of subaerial crust and the onset of
646 a modern hydrologic cycle at 2.5 Ga. Nature 557(7706), 545-548, DOI: 10.1038/s41586-018-
647 0131-1
648 Bindeman, I.N., Bekker, A., Zakharov, D O., 2016. Oxygen isotope perspective on crustal
649 evolution on early Earth: A record of Precambrian shales with emphasis on Paleoproterozoic
650 glaciations and Great Oxygenation Event. Earth Planet. Sci. Lett. 437,101-113. DOI:
651 10.1016/j.epsl.2015.12.029
652 Bowen, G. J., 2019. The Online Isotopes in Precipitation calculator, version 3.1,
653 http://wateriso.utah.edu/waterisotopes/pages/data_access/oipc.html)
654 Bowen, G. J., 2008. Spatial analysis of the intra-annual variation of precipitation isotope ratios
655 and its climatological corollaries. Journal of Geophysical Research 113, D05113,
656 doi:10.1029/2007JD009295.
657 Cappa, C. D., Hendricks, M. B., DePaolo, D. J., Cohen, R. C., 2003. Isotopic fractionation of
658 water during evaporation, J. Geophys. Res., 108(D16), 4525, doi:10.1029/2003JD003597.
659 Dansgaard, W., 1964. Stable isotopes in precipitation. Tellus 16, 436–468.
660 Delgado, A., Reyes, E., 1996. Oxygen and hydrogen isotope compositions in clay minerals: a potential
661 single-mineral geothermometer. Geochim. Cosmochim. Acta 60, 4285–4289.

DePaolo, D.J., Perry, F.V., Baldridge, W.S. 1992. Crustal versus mantle sources of granitic magmas: a two-parameter model based on Nd isotopic studies. Transactions of the Royal Society of Edinburgh: Earth Sciences, 83, 439-446.

Eberl, D.D., 1993. Three zones for illite formation during burial diagenesis and metamorphism. Clay and Clay Minerals 41, 26-37.

Farquhar, J., Wing, B.A., 2005. The terrestrial record of stable sulphur isotopes: a review of the implications for evolution of Earth's sulphur cycle. In: I. McDonald, A.J. Boyce, I.B. Butler, R.J. Herrington, D.A. Polya (Eds.), Mineral Deposits and Earth Evolution, Special Publications, vol. 248, Geological Society, London (2005), pp. 167-177

Gilg, H.A., Girard, J.-P., Sheppard, S.M.F., 2004. Conventinal and less conventional techniques for hydrogen and oxygen isotope analysis of clays, associated minerals and pore waters in sediments and soils. In: Handbook of Stable Isotope Analytical techniques, v. 1, P.A.de Groot (Ed). P. 38-61.

Greber, N.D., Dauphas, N., Bekker, A., Ptáček, M.P., Bindeman, I.N., Hofmann A., 2017. Titanium isotopic evidence for felsic crust and plate tectonics 3.5 billion years ago. Science 357 (6357), 1271-1274.

Hamza, M. S., Epstein, S., 1980. Oxygen isotopic fractionation between oxygen of different sites in hydroxyl-bearing silicate minerals. Geochimica et Cosmochimica Acta 44, 173–182.

Hartmann, J., Moosdorf, N., 2012. The new global lithological map database GLiM: a representation of rock properties at the Earth surface. Geochem. Geophys. Geosyst. 13, Q12004, 1–37.

Hayles, J., Gao, C., Cao, X., Liu,Y., Bao, H., 2018., Theoretical calibration of the triple-oxygen isotope thermometer. Geochim. Cosmochim. Acta 235, 237-245.

Herwartz, D., Surma, J., Voigt, C., Assonov, S., Staubwasser, M., 2017. Triple-oxygen isotope systematics of structurally bonded water in gypsum. Geochim. Cosmochim. Acta 209, 254-266.

Holeman J.N., 1968. The sediment yield of major rivers of the world. Water Resource Research 4, 737-747.

Holland, H.D., 1984. The chemical evolution of the atmosphere and oceans. Princeton University Press. 559p.

Hsieh, J.C.C., Chadwick, O.A., Kelly, E.F., Savin, S.M., 1998. Oxygen isotopic composition of soil water: Quantifying evaporation and transpiration. Geoderma 82, Issues 1–3, P. 269-293.

Kasting, J.F., Howard, M.T., Wallmann, K., Veizer, J., Shields, G., Jaffres, J. 2006. Paleoclimates, ocean depth, and oxygen isotopic composition of seawater. Earth Planet Sci. Lett., 252, 82-93.

Knauth, L.P., Lowe, D.R., 2003. High Archean climatic temperature inferred from oxygen

698 isotope geochemistry of cherts in the 3.5 Ga Swaziland Supergroup, South Africa.
699 Bull. Geol. Soc. Am. 115, 566-580.
700 Land, L.S., Lynch, F.L., 1996. $\delta^{18}O$ values of mudrocks: More evidence for an ^{18}O-buffered
701 ocean. Geochim. Cosmochim. Acta 60, 3347-3352.
702 Lawrence, J.R., Taylor, H.P. Jr. 1971. Deuterium and oxygen-18 correlation: Clay minerals and
703 hydroxides in Quaternary soils compared to meteoric water. Geochim. Cosmochim. Acta 35,
704 993-1003.
705 Li, S., Levin, N. E., Chesson, L. A., 2015. Continental scale variation in 17O-excess of meteoric
706 waters in the United States. Geochim. Cosmochim. Acta 164, 110–126.
707 Luz, B., Barkan, E., 2010. Variations of $^{17}O/^{16}O$ and $^{18}O/^{16}O$ in meteoric waters. Geochim.
708 Cosmochim. Acta 74, 6276–6286.
709 Lyons, T.W., Reinhard, C.T., Planavsky, N.J., 2014. The rise of oxygen in Earth's early ocean
710 and atmosphere. Nature 506 (7488), 307-315.
711 Miller M.F., Pack., A., Bindeman, I.N., Greenwood, R.C. 2019. Standardising the reporting of
712 $\Delta^{17}O$ data from high precision oxygen triple-isotope ratio measurements of silicate rocks and
713 minerals. Chem. Geol. in press.
714 Miller, M. F., 2002. Isotopic fractionation and the quantification of ^{17}O anomalies in the oxygen
715 three-isotope system: an appraisal and geochemical significance. Geochim. Cosmochim.
716 Acta 66, 1881–1889.
717 Mix, H., Chamberlain, C.P., 2014. Stable isotope records of hydrologic change and
718 paleotemperature from smectite in Cenozoic western North America. Geochim.
719 Cosmochim. Acta 141, 532-546.
720 Milliman, J.D., Farnsworth, K.L., 2011. River Discharge to the Coastal Ocean: A Global
721 Synthesis. Cambridge University Press, Cambridge, 143-144.
722 doi.org/10.1017/cbo9780511781247
723 Muehlenbachs, K., 1998. The oxygen isotopic composition of the oceans, sediments and the
724 seafloor: Chemical Geology 145, 263–273.
725 Muehlenbachs, K., Clayton, R.N. 1976. Oxygen isotopic composition of oceanic crust and its
726 bearing on seawater. J Geophys. Res. 81, 4365-4369.
727 Mulch, A., Sarna-Wojcicki, A. M., Perkins, M. E., Chamberlain, C. P., 2008. A Miocene to
728 Pleistocene climate and elevation record of the Sierra Nevada (California). Proc. Natl.
729 Acad. Sci. 105(19), 6819–6824.
730 Nesbitt, H.W., Young, G.M., 1982. Early Proterozoic climates and plate motions inferred from
731 major element chemistry of lutites. Nature 299, 715-717.

Newman, A.C.D., 1987. Chemistry of clays and clay minerals. Mineralogical society monograph series No. 6, Mineralogical society, Longman scientific and technical publisher. 480p. ISBN 0 582 30114 9

Pack, A., Herwartz, D., 2014. The triple-oxygenisotope composition of the Earth mantle and understanding $\Delta^{17}O$ variations in terrestrial rocks and minerals. Earth Planet. Sci. Lett. 390, 138–145.

Pack, A., Tanaka R., Hering, M., Sengupta, S., Peters, S. Nakamura, E., 2016. The oxygen isotope composition of San Carlos olivine on the VSMOW2-SLAP2 scale. Rapid Communications to Mass Spectrometry 30, 1495-1504.

Parai, R., Mukhopadhyay S., 2012. How large is the subducted water flux? New constraints on mantle regassing rates. Earth Planet. Sci. Lett. 317-318, 396-406.

Passey, B.H., Ji, H., 2019. Triple-oxygen isotope signatures of evaporation in lake waters and carbonates: A case study from the western United States. Earth Planet. Sci. Lett. 518, 1–12.

Pettijohn, F.J., 1957. Sedimentary Rocks, second edition. Harper, New York, 718 pp.

Rozanski, R., Araguás-Araguás L., Gonfiantini R., 1993. Isotopic Patterns in Modern Global Precipitation. In P. K. Swart, K. C. Lohmann, J. Mckenzie andS. Savin Eds. Climate Change in Continental Isotopic Records, Geophysical Monograph 78, p. 1-36.

Retallack, G.J., 2001. Soils of the past. an Introduction to Pedology, Blackwell Science, Oxford, ed. second, p. 404.

Ronov, A. B., Yaroshevsky, A. A., 1969. Chemical Composition of the Earth's Crust, in The Earth's Crust and Upper Mantle, ed P. J. Hart, American Geophysical Union, Washington, D. C., doi: 10.1029/GM013p0037

Rudnick, R.L., Gao, S., 2003. Composition of the continental crust- Treatise on geochemistry, olume 3. Editor: Roberta L. Rudnick. Executive Editors: Heinrich D. Holland and Karl K. Turekian. 659 p. ISBN 0-08-043751-6. Elsevier, pp. 1-64

Savin, S., Epstein, S. 1970a. The oxygen and hydrogen isotope geochemistry of clay minerals. Geochim. Cosmochim. Acta 34, 25-42.

Savin, S., and Epstein, S., 1970b. The oxygen and hydrogen isotope geochemistry of ocean sediments and shales. Geochim. Cosmochim. Acta 34, 43-63.

Savin, S.M., Hsieh, J.C.C., 1998. The hydrogen and oxygen isotope geochemistry of pedogenic clay minerals: principles and theoretical background. Geoderma 82, 227-253.

Savin, S. M., Lee M. L., 1988. Isotopic studies of phyllosilicates. Reviews in Mineralogy and Geochemistry 19, 189–223.

Silverman, S.R., 1951. The isotope geology of oxygen. Geochim. Cosmochim. Acta. 39, 5669-584.

767 Simon, L., Lécuyer, C. 2005. Continental recycling: The oxygen isotope point of view.
768 Geochemistry, Geophysics, Geosystems 6 (8), doi:10.1029/2005GC000958.
769 Shackleton, N.J., Kennett, J.P., 1975. Paleotemperature history of the Cenozoic and the
770 initiation of Antarctic glaciation; oxygen and carbon isotope analyses in DSDP sites
771 277, 279 and 281. Initial Rep. Deep Sea Drill. Proj. 29, 743–755.
772 Sharp, Z. D., Gibbons, J. A., Maltsev, O., Atudorej,V., Pack, A., Sengupta, S., Shock, E. L.,
773 Knauth, L. P., 2016. A calibration of the triple-isotope fractionation in the SiO_2–H_2O system
774 and applications to natural samples. Geochim. Cosmochim. Acta 186, 105–119.
775 Sharp, Z. D., Wostbrock, J. A. G. and Pack, A. 2018. Mass-dependent triple-oxygenisotope
776 variations in terrestrial materials. Geochem. Persp. Lett. 7, 27–31.
777 Shaw, D.B., Weather, C.E., 1965. The mineralogical composition of shales. J. Sed. Petrol. 35,
778 213-222.
779 Sheppard, S.M.F., Gilg, H.A., 1996. Stable isotope geochemistry of clay minerals. Clay Minerals
780 31, 1-24.
781 Seligman, A.N., Bindeman, I.N., 2019. The $\delta^{18}O$ of primary and secondary waters in hydrous
782 volcanic glass. J. Volcanol. Geotherm. Res. 371, 72-85.
783 Sengupta, S., Pack, A., 2018. Triple oxygen isotope mass balance for the Earth's oceans with
784 application to Archean cherts. Chem Geol. 495, 18-26.
785 Uemura, R., Barkan, E., Abe, O. and Luz, B., 2010. Triple-isotope composition of oxygen in
786 atmospheric water vapor. Geophys. Res. Lett. 37, L04402.
787 Yeh, H.-W., Savin, S.M., 1976. The extent of oxygen isotope exchange between clay minerals
788 and sea water. Geochim. Cosmochim. Acta 40, 743-748.
789 Yeh, H.-W., and Savin, S.M., 1977. Mechanism of burial metamorphism of argillaceous
790 sediments: 3. O-isotope evidence. GSA Bulletin 88 (9), 1321-1330.
791 Wedepohl, K.H., 1995. The composition of the continental crust. Geochimica et Cosmochimica
792 Acta 59, 1217-1239. doi: 10.1016/0016-7037(95)00038-2.
793 Zakharov, D.O., Bindeman, I.N., 2019. Triple oxygen and hydrogen isotopic study of
794 hydrothermally altered rocks from the 2.43-2.41 Ga Vetreny belt, Russia: An insight into
795 the early Paleoproterozoic seawater. Geochim. Cosmochim. Acta 248, 185-209.
796 Zheng, Y.F., 1993a. Calculation of oxygen isotope fractionation in anhydrous silicate minerals;
797 Geochim. Cosmochim. Acta 57, 1079-1091.
798 Zheng, Y.F., 1993b. Calculation of oxygen isotope fractionation in hydroxyl-bearing silicates.
799 Earth. Plan. Sci. Lett. 120, 247-263.
800
801
802

Figure Captions

Fig. 1. a) Studied river basins superimposed on the world isotopic precipitation map (waterisotopes.org), showing that our sample collection covers most of the modern environments of weathering from tropical to Arctic, and from wet to arid. Each sample collection site is shown by a symbol indicating predominant watershed bedrock type. Numbers correspond to river names in Table A1. XRD-determined clay proportions for selected rivers is shown; see Fig. A2 for others.

b). Compiled data for $\delta^{18}O$ values of water in studied rivers plotted vs MAT for watershed basins (Table A1). Notice that the best fit lines (dashed and dotted) are nearly coincident with the global meteoric water datasets for precipitation from Bowen (2008, linear), and Rozanski et al. (1993, quadratic) fits.

Fig. 2. Computed $^{18}O/^{16}O$ isotope fractionations vs. temperature.

a) Clay-water fractionation factors, "bulk" clay is the weighted average of world clays based on XRD proportions for studied clays measured here with: 34% smectite, 29% illite, 22% kaolinite, and 15% chlorite. Data is from Sheppard and Gilg (1996, most clays), (Savin and Lee, 1988, chlorite) and Sharp et al. (2016, quartz).

b) The $\delta^{18}O$ of clays in equilibrium with meteoric water that follows the global $\delta^{18}O$ -MAT relationship in Fig. 1b. Notice that due to the opposing effects of T on the $\delta^{18}O$ of MW and fractionation, there is significant $\delta^{18}O$ clay overlap above ~15°C. Corresponding $\Delta^{17}O$(Clay-MW) vs. MAT graph is plotted in Fig. A1.

Fig. 3. Relationships between $\delta^{18}O$ of studied clays, silts and sands and their respective Chemical Index of Alteration, CIA. Clay samples show scatter and no trends with CIA, while silts with smaller CIA have more detrital, and water-poor compositions. Note that silt $\delta^{18}O$ and CIAs do still extend to high values, because they also contain significant weathering products. CIA data is derived from separate chemical analyses of clays and silts by Bayon et al. (2016, 2018) for the same samples, for sand water-based estimate is used.

Fig. 4. The $\delta^{18}O$ oxygen isotopic compositions of clays and silt-sized fractions, and water in clays (WIC) as a function of MAT. Each vertical array represents a single sample. Notice no correlation with MAT for clays and WIC, and a subtle positive correlation for silts, explained by greater proportion of detrital components in cold climates with greater physical weathering proportions. Silts and clays overlap in tropical climates.

Fig. 5. Isotopic fractionation between studied clays, local mean annual isotopic precipitation (MW) vs. Mean Annual Temperature of their respective watersheds. Each vertical array represents a single sample.

a) $\Delta^{18}O$(Clay-MW), showing that isotopic fractionation is expectedly decreasing with increasing temperatures parallel to the computed fractionation relations (solid black line) from **Fig. 2a**. The ~2‰ offset is explained by a lower $\delta^{18}O$ detrital contribution. Maroon symbols indicate water-in-clay (WIC) $\delta^{18}O$ values, which also decrease with increasing temperature, maintaining similar ~-8‰ offset relative to bulk clay values.

b) The $\Delta\Delta'^{17}O$(Clay-MW) vs temperature showing similar relationships. The offset with fit parameters is also explained by detrital dilution of clays. See text for discussion.

Fig. 6. The oxygen isotopic compositions of clays and computed weathering product as a function of MAT. Each vertical array represents a single sample.

879 a) $\delta^{18}O$ of clays and computed weathering product (WP) based on the linear mass balance
880 formula Eqs. [11]-[12] in the text, exhibiting little global trend. It is explained by the
881 counterbalancing effects of temperature on $\delta^{18}O_{MW}$, and on isotopic fractionation (**Figs. 1b and**
882 **2a**): at low temperatures e.g. subarctic, there is a greater $\Delta^{18}O_{clay\text{-}water}$ fractionation factor (**Fig. 2**),
883 but meteoric water also tends to be lighter (**Fig. 1**), thereby explaining the trend towards lower
884 $\delta^{18}O_{weathering\ product}$. In contrast, tropical regions are characterized by heavier $\delta^{18}O_{MW}$
885 compositions, but this effect is hampered by small $\Delta^{18}O_{clay\text{-}water}$ fractionation factors at high
886 temperatures (**Fig. 2**), again leading to lighter $\delta^{18}O_{weathering\ product}$. $\delta^{18}O_{WIC}$ data is also shown and
887 exhibit no trend with MAT.
888 b) $\Delta'^{17}O_{clay}$, showing a linear relationships for clays and weathering products.
889
890 Fig. 7. Triple-oxygen isotopes for clays from world rivers plotted for mean annual temperature of
891 weathering conditions in their respective watersheds (data from Table A1). Clay-water
892 fractionation lines (Eqs. 9-10), are emanating from parental weathering waters. Note the
893 significant overlap of clay triple-oxygen values from different climates, broadly explained by
894 relationships shown on **Figs. 2b**, and **4**. Clays from modern world representing modern oxygen
895 isotopic diversity of weathering products with average temperatures and continental sizes,
896 overlap with field from post-Archean shales (from Bindeman et al. 2018). This advocates for
897 comparable $\delta^{18}O_{MW}$ and surface temperatures (inset showing Effects) and overall hydrologic
898 conditions of weathering, since post-Archean. These two parameters are primarily responsible
899 for spread of data points on this graph. The concave down yellow curve denotes mixing of
900 weathering products with detrital crustal material. Two water lines (MWL, Luz and Barkan,
901 2010, and WW) are shown, different by a constant $\Delta'^{17}O$ of 0.033, explained by the extent of
902 evaporation of water participating in weathering in soils (small vector under Effects, e.g. Surma
903 et al. 2018; Passey and Ji, 2019). Clay-water fractionation curvature is likely greater than for
904 Quartz-water (Sharp et al. 2016), explained by a parameter *s* in Eq. 10, see inset to the right, and
905 text for discussion. The tropical curve is for MAT>20°C, the arctic for T<5°C, the temperate is
906 for 5-19°C; dry is for MAP <760mm/yr, wet is for MAP>1000mm/yr, with data in Table A1.
907 Sand and Silt average represent measured values (Table 1) for global composite samples,
908 weighted by the sediment flux.
909
910 **Fig. 8.** Computed vs. measured temperatures (a) and $\delta^{18}O$ values of meteoric waters (b) based on
911 triple-oxygen isotopic composition of weathering products. These data are plotted on the $\delta^{18}O$ vs
912 T relationship (c) and are compared to global fit lines for modern waters (see **Fig. 1b**). Note that
913 computed values agree within ~10°C and ~5‰, but give an $\delta^{18}O$-T correlation with a slope and
914 range equal to the global dataset with an offset. Blue lines connect individual samples. Grey field

in c denotes variations *s* in the slope of ^{17}O fractionation, to 2.05 as per Eq.10 leading to somewhat better fractionation. See text for discussion and Fig. A6 for further analysis. Only data with solved roots of analytical inversion are plotted (~90% of data), other data points returned unrealistically low or high values, e.g. T <<0°C and $\delta^{18}Ow$ of >>0‰, or <<20‰.

Data Availability Statement

Data is available in Excel format as a part of this publication (Online Figures A1-A6 and Tables A1-A3)

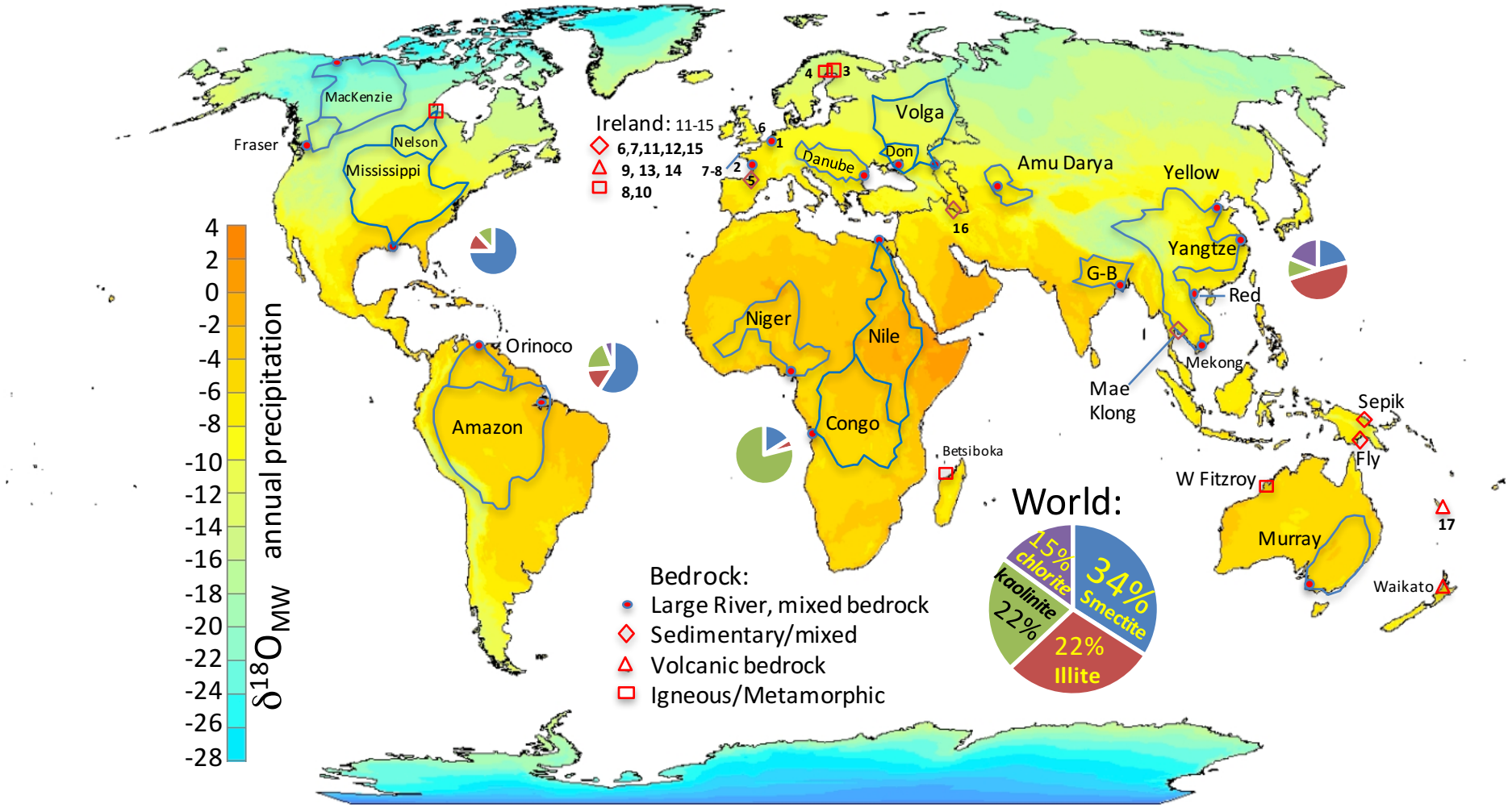
MacKenzie
Fraser
Nelson
Mississippi
Orinoco
Amazon
Niger
Nile
Congo
Betsiboka
Volga
Don
Danube
Amu Darya
Yellow
Yangtze
G-B
Red
Mekong
Mae Klong
Sepik
Fly
W Fitzroy
Murray
Waikato
17
16
Ireland: 11-15
6,7,11,12,15
9, 13, 14
8,10
7-8
4
3
6
1
2
5
4
2
0
-2
-4
-6
-8
-10
-12
-14
-16
-18
-20
-22
-24
-26
-28
δ18OMW annual precipitation
Bedrock:
Large River, mixed bedrock
Sedimentary/mixed
Volcanic bedrock
Igneous/Metamorphic
World:
34% Smectite
22% Illite
22% kaolinite
15% chlorite

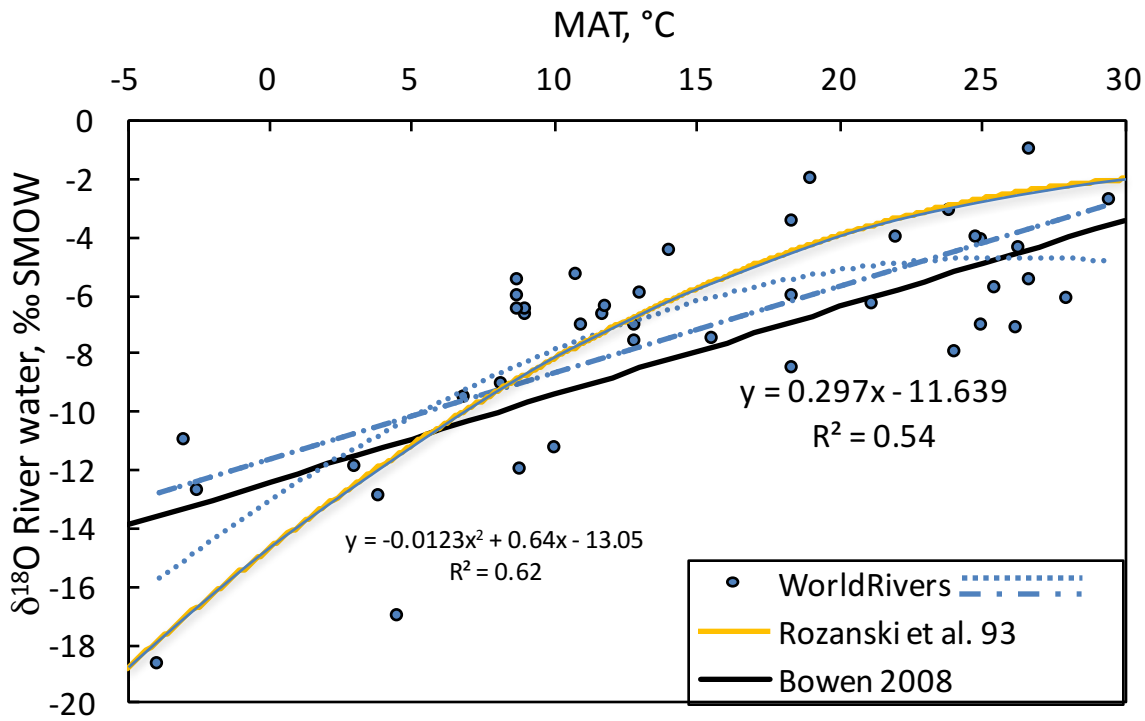
MAT, °C
-5
0
5
10
15
20
25
30
0
-2
-4
-6
-8
-10
-12
-14
-16
-18
-20
δ18O River water, ‰ SMOW
y = 0.297x - 11.639
R² = 0.54
y = -0.0123x² + 0.64x - 13.05
R² = 0.62
WorldRivers
Rozanski et al. 93
Bowen 2008

Fig 1b

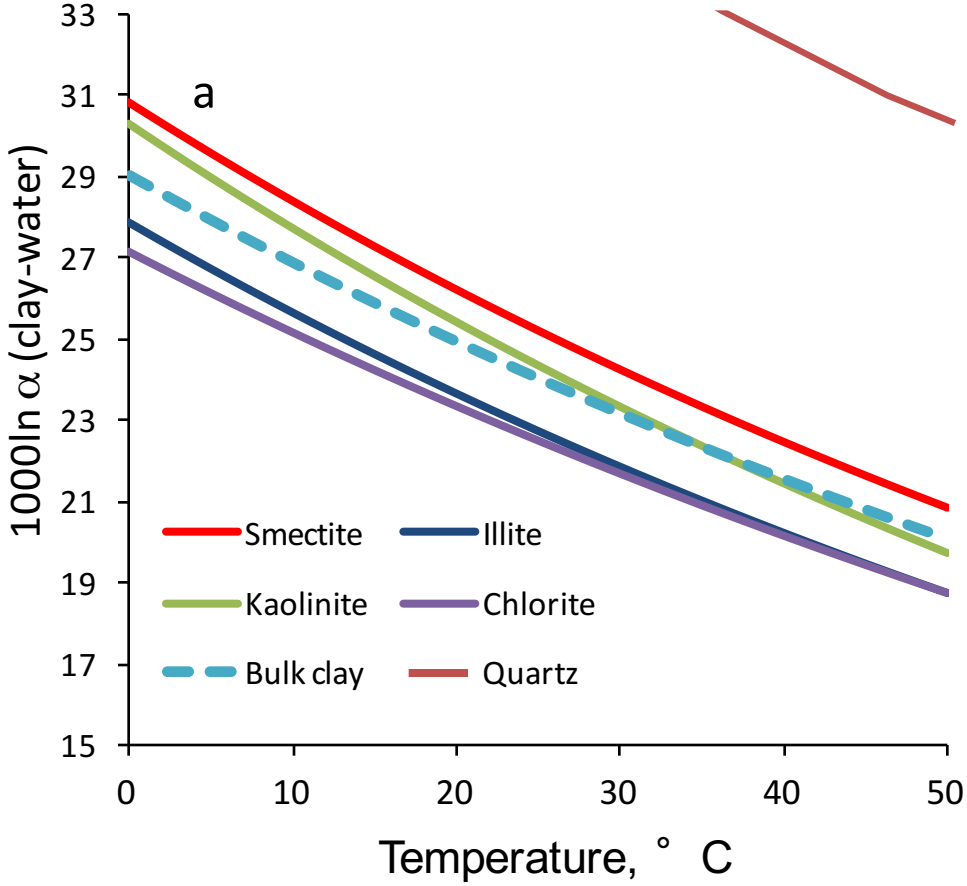
a
1000ln α (clay-water)
33
31
29
27
25
23
21
19
17
15
0
10
20
30
40
50
Temperature, ° C
Smectite
Illite
Kaolinite
Chlorite
Bulk clay
Quartz

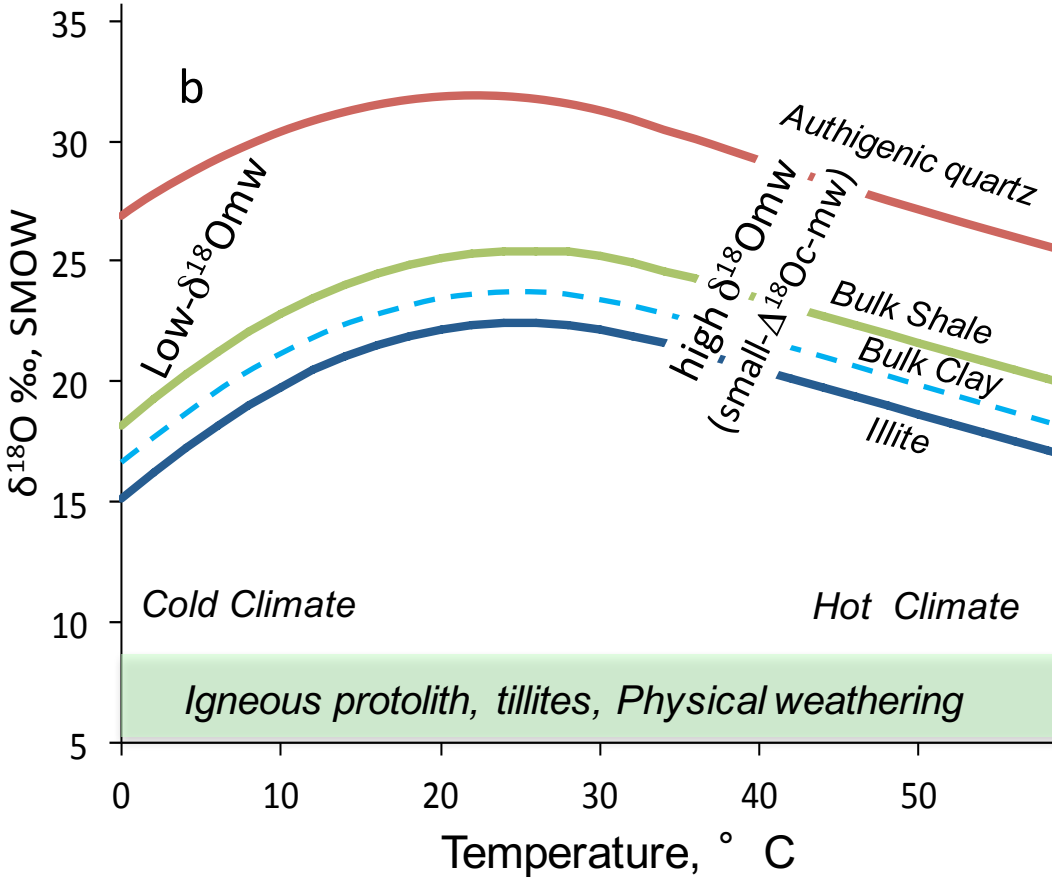
b
δ18O ‰, SMOW
35
30
25
20
15
10
5
0
10
20
30
40
50
Temperature, ° C
Authigenic quartz
Low-δ18Omw
high δ18Omw
(small-Δ18Oc-mw)
Bulk Shale
Bulk Clay
Illite
Cold Climate
Hot Climate
Igneous protolith, tillites, Physical weathering

Fig 2

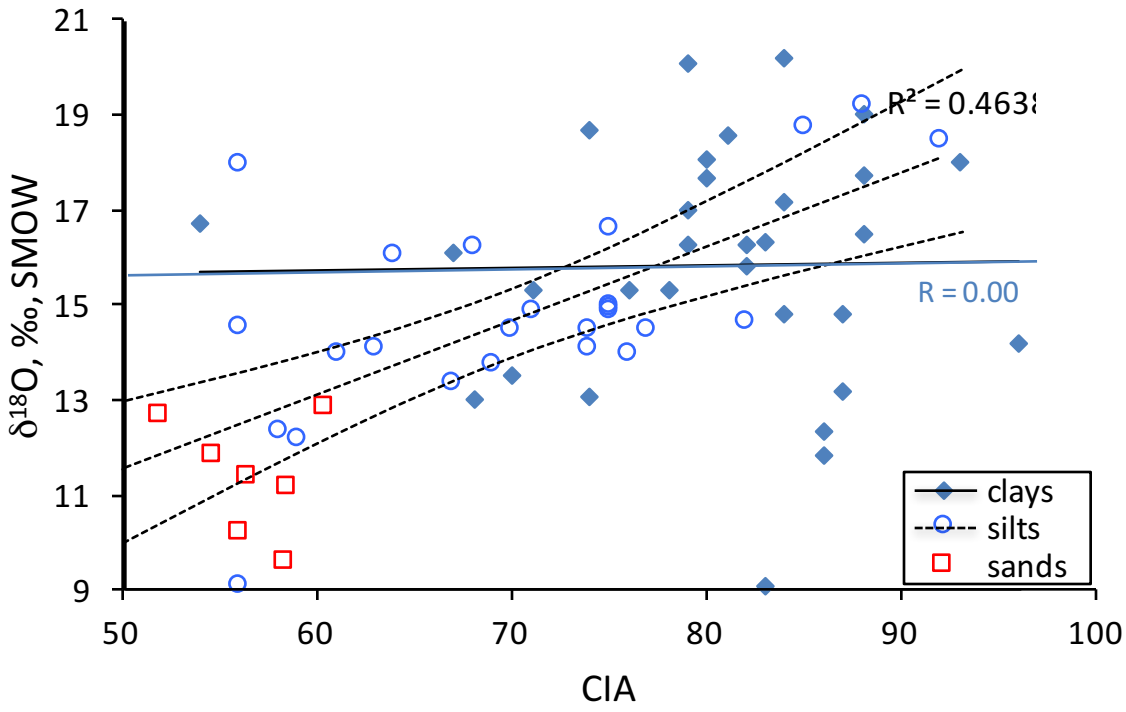
21
19
17
15
13
11
9
δ18O, ‰, SMOW
50
60
70
80
90
100
CIA
R² = 0.463
R = 0.00
clays
silts
sands

Fig 3

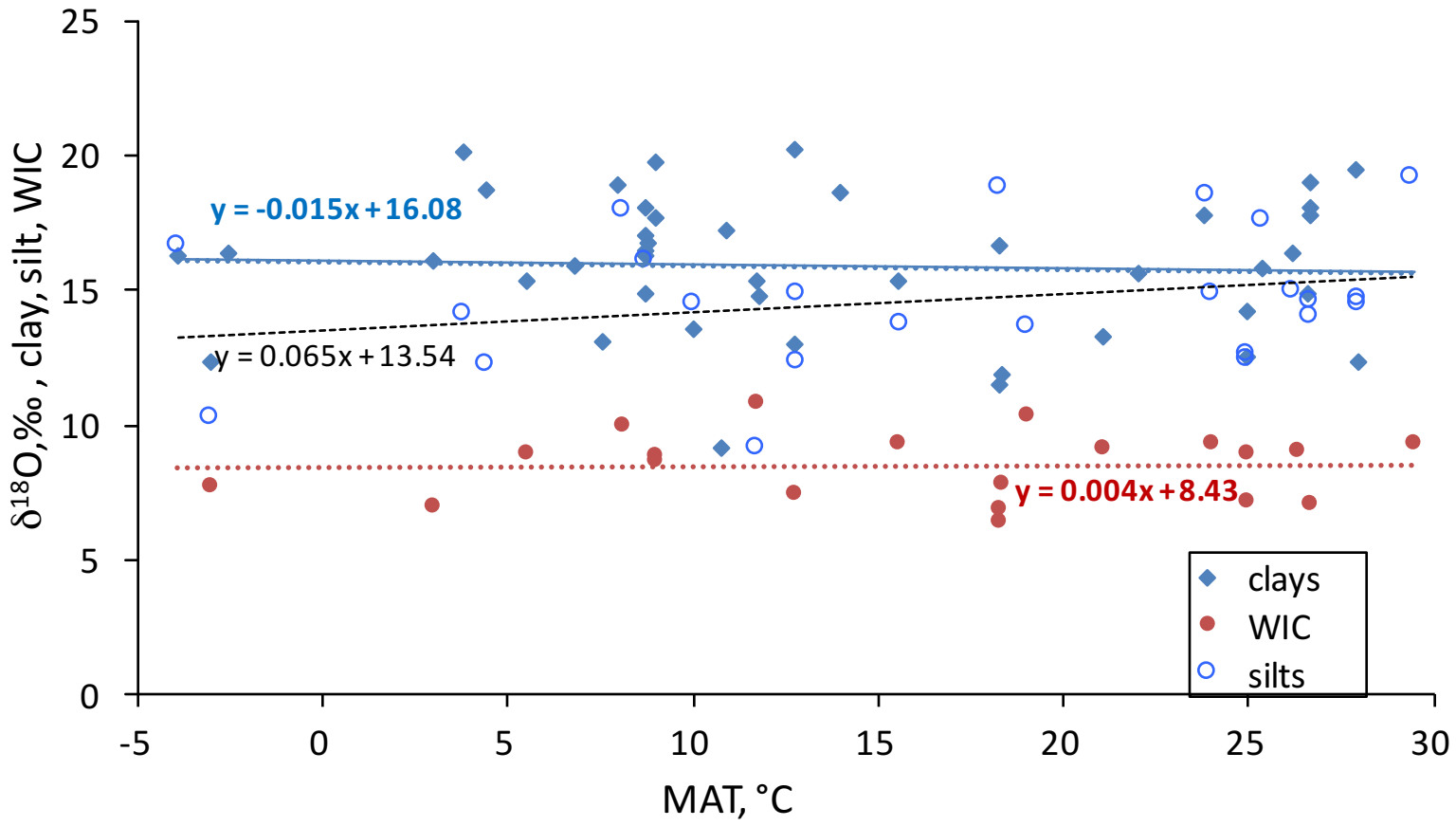
25
20
15
10
5
0
-5
0
5
10
15
20
25
30
δ18O,‰, clay, silt, WIC
MAT, °C
y = -0.015x + 16.08
y = 0.065x + 13.54
y = 0.004x + 8.43
clays
WIC
silts

Fig 4

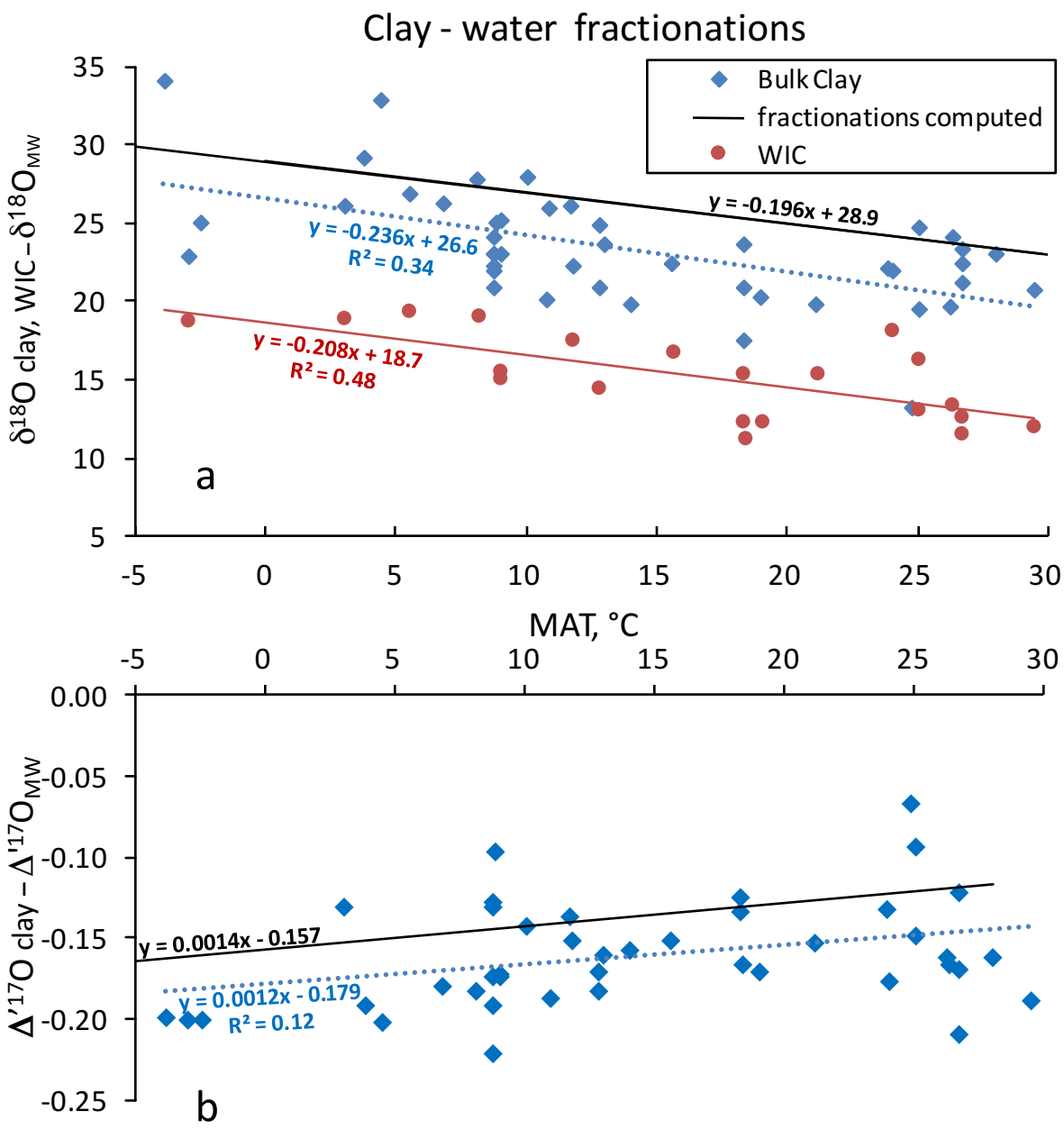
Clay - water fractionations
Bulk Clay
fractionations computed
WIC
y = -0.196x + 28.9
y = -0.236x + 26.6
R² = 0.34
y = -0.208x + 18.7
R² = 0.48
a
δ18O clay, WIC – δ18OMW
MAT, °C
y = 0.0014x - 0.157
y = 0.0012x - 0.179
R² = 0.12
b
Δ'17O clay – Δ'17OMW

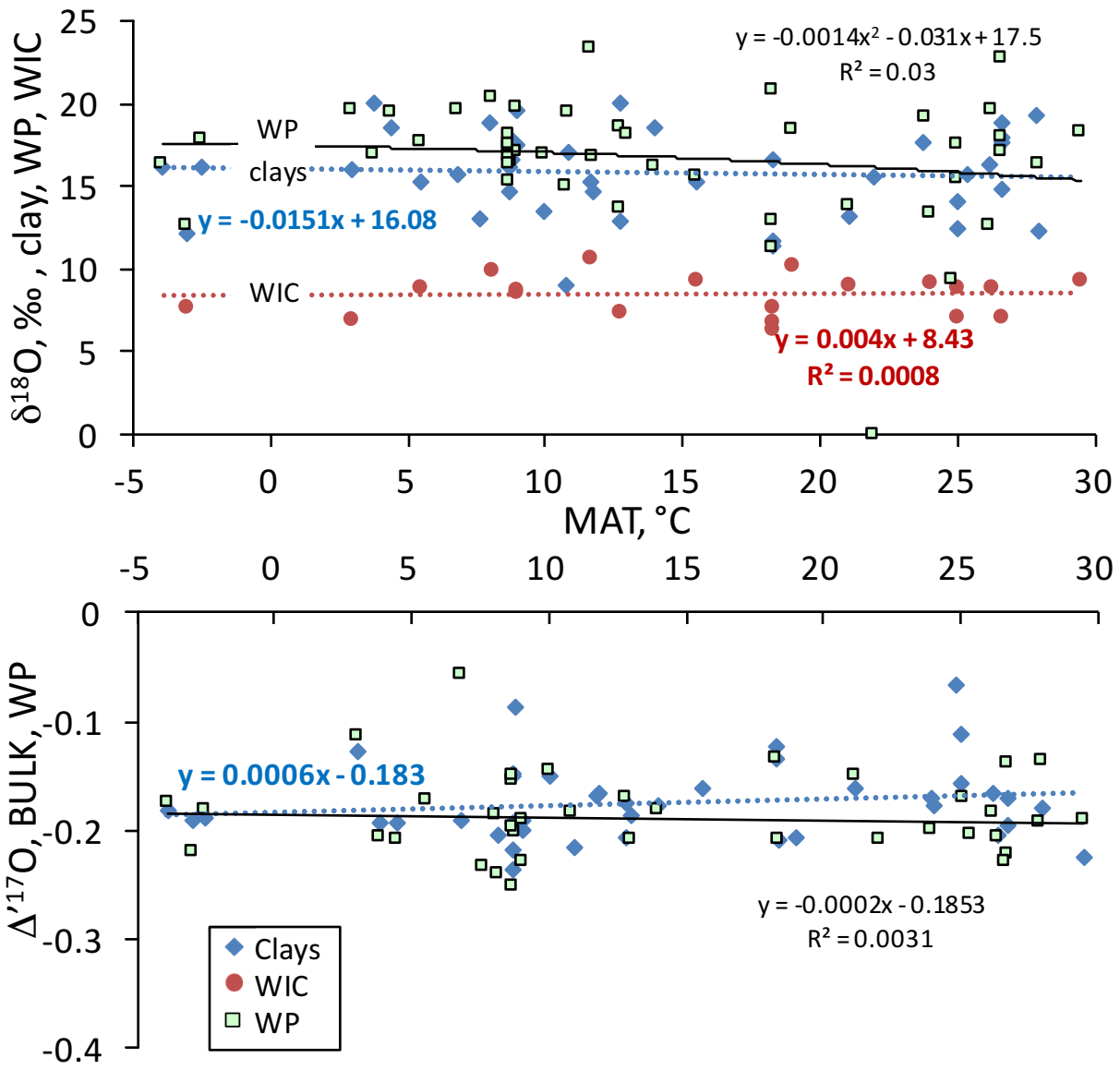
y = -0.0014x² - 0.031x + 17.5
R² = 0.03
WP
clays
y = -0.0151x + 16.08
WIC
y = 0.004x + 8.43
R² = 0.0008
δ18O, ‰ , clay, WP, WIC
MAT, °C
y = 0.0006x - 0.183
y = -0.0002x - 0.1853
R² = 0.0031
Δ'17O, BULK, WP
Clays
WIC
WP

Fig. 6

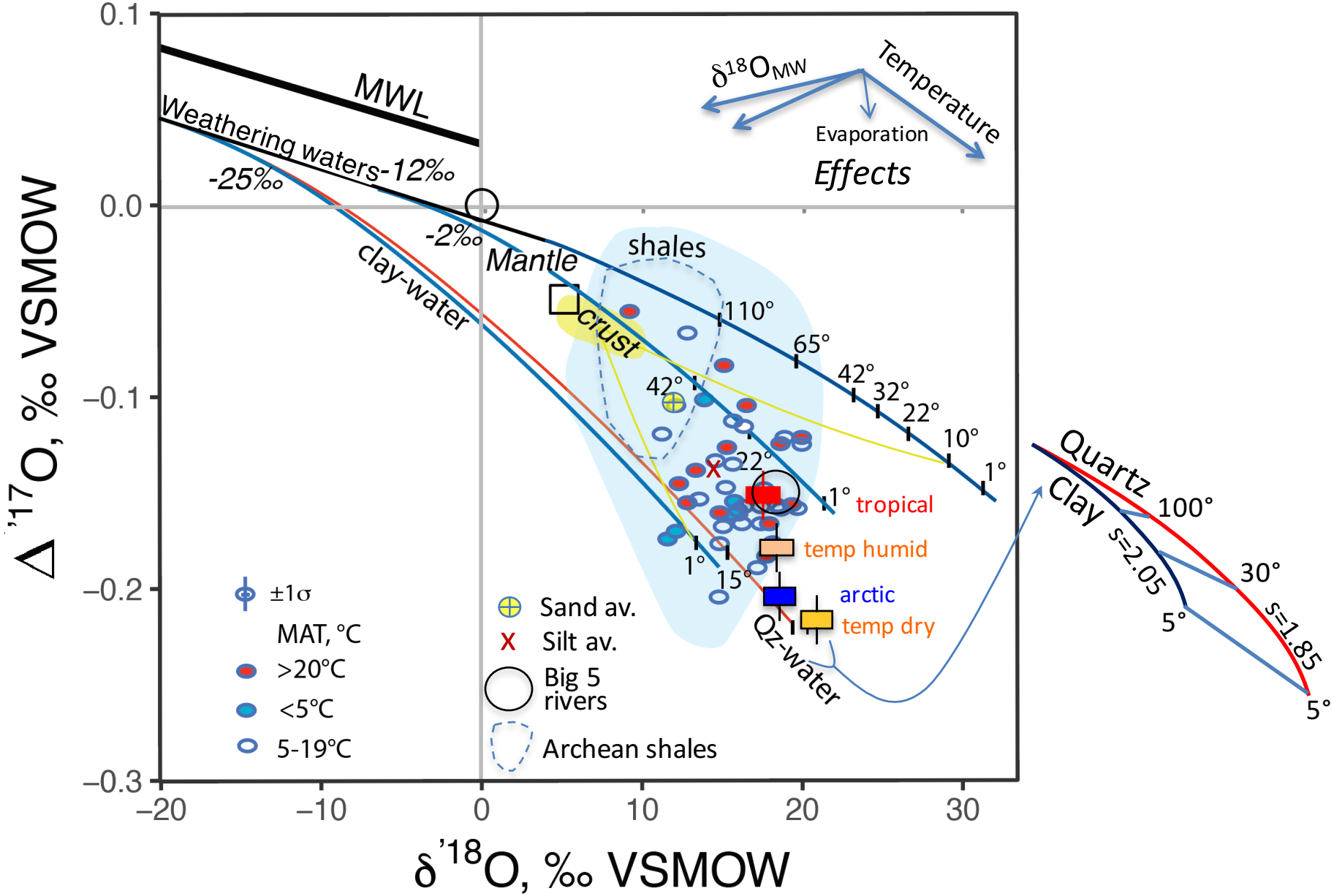
MWL
Weathering waters-12‰
-25‰
-2‰
clay-water
Mantle
crust
shales
110°
65°
42°
32°
22°
10°
1°
42°
22°
1°
15°
1° tropical
temp humid
arctic
temp dry
QZ-water
Quartz
Clay
100°
30°
5°
s=2.05
s=1.85
5°
δ18OMW
Temperature
Evaporation
Effects
±1σ
MAT, °C
>20°C
<5°C
5-19°C
Sand av.
Silt av.
Big 5 rivers
Archean shales
Δ'17O, ‰ VSMOW
δ'18O, ‰ VSMOW
0.1
0.0
–0.1
–0.2
–0.3
–20
–10
0
10
20
30

Fig. 7

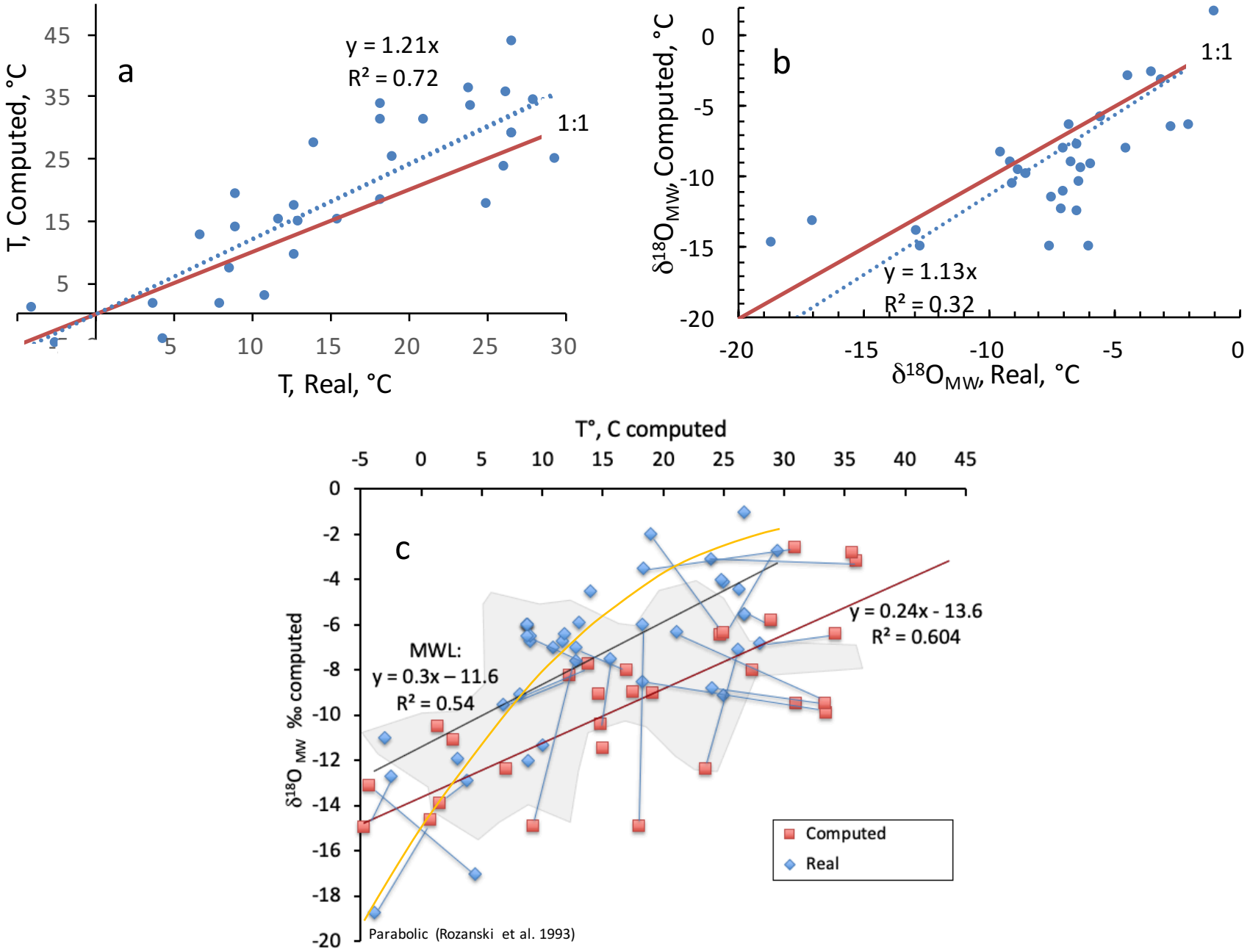
a
y = 1.21x
R² = 0.72
1:1
T, Computed, °C
T, Real, °C
b
1:1
y = 1.13x
R² = 0.32
δ18OMW, Computed, °C
δ18OMW, Real, °C
c
T°, C computed
MWL:
y = 0.3x – 11.6
R² = 0.54
y = 0.24x - 13.6
R² = 0.604
Computed
Real
Parabolic (Rozanski et al. 1993)
δ18O MW ‰ computed

Fig. 8

Table 1 Oxygen isotope values of modern crust and surface

	Surface	Upper Crust	$\delta^{18}O$	$\delta^{18}O$	$\Delta'^{17}O$	Ref
Global Lithological Types	GLiM^	W95^	SL_05^	this work	this work	
Metamorphic	0.15	0.3	8.66	8.66	-0.07	2
Igneous Crustal	0.136	0.3	9.4	9.4	-0.065	2
Igneous Basic	0.028	0.288	6.13	6.13	-0.055	1
Sedimentary, including:	0.686	0.112	14	14.9 (14.2 silicate)		
Limestones, marls*	*0.079*	*0.020*	25.8	*21.5*	-0.08	2
Sandstones	0.192	0.030	11	11	-0.075	4
Conglomerates	0.036			8	-0.06	4
Shale	0.458	0.063	15	14.6	-0.154	3
Silt, composite sample				14.08	-0.135	10
water in clay				8.5±1.2		7
Global Average	1.000					
Upper Crust		1.00	9.62	9.62	-0.070	5
Lower crust			8.1	8.1	-0.063	6
Silicate Surface				11.83	-0.108	5
Surface with limestone				12.60	-0.106	5
Other silicate surface estimates from this work:						
Sand from 7 major rivers, average				11.38±1.1		8
Sand, composite sample				11.98	-0.101	10
Silt projected to CIA=50				11.57±1		8
Glacial tillites				11.5±2.9		9
Ignimbrites				10±2	-0.100	9
Accepted silicate surface:				11.5±1	-0.108	9

*excluded from computing silicate weathering flux; can be isotope flux neutral if bulk δ18Ocarb = +21.5‰

^GLiM: Hartmann and Moosdorf, 2012; SL_05: Simon and Lecuyer 2005, W95: Wedepohl (1995).

1-Δ'17O value based on mantle value of Pack et al. (2016); 2-Sharp et al. (2018); 3- Bindeman et al. (2016, 2018 average of post-Archean non-glacial shale, n=123; 4-detrital-authigenic mix; 5-based on this Table;

6- rock proportions: 1/3 each metamorphic, igneous basic and silicic;

7- δ18O of water extracted by pyrolysis, Fig. 4 ; 8- see Fig. 3; 9 -see section 4.2 in text for discussion

10- global composite made using weighted proportions of sediment flux per region (Table 2)

Table 2. Estimating global weathering fluxes weighted by the amount of weathering in different regions
Weathering bedrock has δ18O= +11.5‰ and Δ17O = -0.125‰ (Δ'17O=-0.108‰), Table 1

				average weighted values					*weathering flux*			*Weathering products*	
Region	flux , Gt/yr	% global	River	$\delta^{18}O_{MW}$ ‰	MAT °C	$\delta^{18}O_{clay+silt}$ (TSS), ‰	$\delta^{18}O_{clay}$ ‰	$\Delta^{17}O_{clay}$ ‰	$\Delta\delta^{18}O$, ‰	flux/% global C x K ‰ Gt	$\Delta\Delta^{17}O$, ‰	$\delta^{18}O_{WP}$, ‰	$\Delta^{17}O_{WP}$, ‰
		C				K			@11.5‰		@-0.125‰	computed, TSS-weighted	
Indonesia	2700	0.141	Sepik, Fly, Brantas, Mekong, Red, Mae Klong	-7.6	24.9	14.31	14.15	-0.168	2.81	0.3968	-0.0060	15.29	-0.1802
Papua	1700	0.089	Sepik, Fly, Brantas	-8.1	25.6	13.69	14.04	-0.161	2.19	0.1947	-0.0032	15.99	-0.1795
SE Asia	2600	0.136	Mekong, Red, Mae Klong, Chao Praya	-7.3	24.4	14.72	14.22	-0.172	3.22	0.4382	-0.0064	14.62	-0.1806
China	2240	0.117	Yellow, Yangtze, Red	-8.0	17.5	13.62	13.70	-0.171	2.12	0.2483	-0.0054	14.27	-0.1887
India, Pakistan	2600	0.136	Ganges, Brahmaputra	-7.3	18.3	12.02	11.85	-0.129	0.52	0.0708	-0.0006	12.16	-0.1401
S America Amazon	1430	0.075	Amazon	-5.5	26.7	14.41	17.70	-0.196	2.91	0.2178	-0.0053	18.00	-0.2100
Africa	950	0.05	Nile, Niger, Congo	-3.1	27.6	17.68	19.06	-0.197	6.18	0.3090	-0.0036	20.14	-0.1981
Others (Global Av)	5830	0.255	all other average	-7.9	13.5	14.29	16.13	-0.175	2.79	0.7121	-0.0126	17.47	-0.1961
Global Sum	19100	**1.000**	*Sediment flux-weighted global averages:*	***-7.3***	***20.5***	***14.09***	***14.80***	***-0.164***	Total silicate	**2.59**	**-0.0432**	**17.39**	**-0.1829**